

**SIMULATIONS OF THE MAGNETIZATION AND
MAGNETOVISCOSECITY OF DILUTE MAGNETIC FLUIDS**

By
Jorge Hernán Sánchez Toro

A thesis submitted in partial fulfillment of the requirements for the degree of

DOCTOR OF PHILOSOPHY

In

CHEMICAL ENGINEERING

UNIVERSITY OF PUERTO RICO
MAYAGÜEZ CAMPUS

2009

Approved by:

Carlos Rinaldi, PhD
President, Thesis Committee

Date

Julio G. Briano, PhD
Member, Thesis Committee

Date

Aldo Acevedo, PhD
Member, Thesis Committee

Date

Patricia Ortiz, PhD
Member, Thesis Committee

Date

Astrid Cruz, PhD
Graduate Studies Representative

Date

David Suleiman, PhD
Chair, Chemical Engineering

Date

ABSTRACT

In this work was studied the rotational Brownian motion of magnetic spherical and tri-axial ellipsoidal particles suspended in a Newtonian fluid, in the dilute suspension limit, under applied shear and magnetic fields by Brownian dynamics simulation to determine the magnetization and magnetoviscosity of the suspension. The algorithm describing the change in the magnetization and magnetoviscosity of the suspension was derived from the stochastic angular momentum equation using the fluctuation-dissipation theorem and a quaternion formulation of orientation space. Results are presented for the response of dilute suspensions of magnetic nanoparticles to constant and transient magnetic fields with and without simple shear flow fields.

Simulation results are in agreement with the Langevin function for equilibrium magnetization and with single-exponential relaxation from equilibrium at small fields using Perrin's effective relaxation time. Dynamic susceptibilities for ellipsoidal particles of different aspect ratios were obtained from the response to oscillating magnetic fields of different frequencies and described by Debye's model for the complex susceptibility using Perrin's effective relaxation time.

Suspensions of ellipsoidal particles show a significant effect of aspect ratio on the intrinsic magnetoviscosity of the suspension, and this effect is more pronounced as the aspect ratio becomes more extreme. The use of an effective rotational diffusion coefficient $D_{r,eff}$ collapses the normalized intrinsic magnetoviscosity of all suspensions to a master curve as a function of Péclet number and the Langevin parameter $\alpha = (\mu_0 \mu H) / (k_B T)$, up to a critical value of α for which the results for suspensions of

spherical particles deviate from those of suspensions of ellipsoids. This discrepancy is attributed to the action of the shear-torque on the ellipsoidal particles, which tends to orient the particles in the direction of maximum deformation of the simple shear flow.

On the other hand, for suspensions of spherical particles a decrease to negative values in the intrinsic magnetoviscosity is observed for oscillating and co-rotating magnetic fields whereas an increase is observed for counter-rotating magnetic fields. The frequency corresponding to zero viscosity and the minimum value in the negative viscosity is lower for co-rotating magnetic fields than for oscillating magnetic fields. In the negative magnetoviscosity regions the particles in a co-rotating magnetic field rotate faster than in an oscillating magnetic field. It is estimated that the flow due to co-rotating particles could be strong enough to obtain a negative effective viscosity in dilute suspension. Moreover, it is shown that the commonly accepted constitutive equation for the antisymmetric stress describes well the intrinsic magnetoviscosity of the suspension.

ACKNOWLEDGEMENTS

I want to dedicate this achievement to all those who were with me at this stage of my life: Maik Irrazabal, Dennise Soto, Ana Arevalo, Lilia Olaya, Ana M. Gonzalez, Alexar Pol, and Dr. Miguel Pando, for their help and friendship; and very specially to Victoria L. Calero for her love and patience.

To my parents, Jorge and Gloria, and to my brothers, Pilar, Mario, and Beto, for their love and trust in the distance.

I thanks to my advisor Dr. Carlos Rinaldi for his support and scientific vision of the work, and to Dr. Julio Briano for his advice and those long talks about life.

This work was supported by the US National Science Foundation CAREER program (CBET-0547150)

CONTENT

1	INTRODUCTION.....	1
1.1	MAGNETIC FLUIDS	1
1.2	MAGNETIC PROPERTIES OF FERROFLUIDS.....	2
1.2.1	<i>Equilibrium magnetization and Langevin function.....</i>	<i>2</i>
1.2.2	<i>Dynamic magnetization and Debye model</i>	<i>6</i>
1.3	RHEOLOGICAL PROPERTIES	11
1.4	ROTATIONAL BROWNIAN MOTION OF AN ORTHOTROPIC PARTICLE IN MAGNETIC AND SHEAR FIELDS	13
1.5	MOTIVATION.....	21
2	ROTATIONAL BROWNIAN DYNAMICS SIMULATIONS OF NON- INTERACTING MAGNETIZED ELLIPSOIDS PARTICLES IN CONSTANT AND OSCILLATING MAGNETIC FIELDS.....	25
2.1	CALCULATION OF THE MAGNETIZATION OF THE SUSPENSION.....	28
2.2	MAGNETIZATION RESPONSE TO WEAK MAGNETIC FIELDS	29
2.2.1	<i>Simulation parameters.....</i>	<i>29</i>
2.2.2	<i>Simulation results and discussion.....</i>	<i>30</i>
2.3	MAGNETIZATION RESPONSE TO STRONG MAGNETIC FIELDS	38
2.3.1	<i>Simulation parameters.....</i>	<i>40</i>
2.3.2	<i>Simulation results and discussion.....</i>	<i>40</i>
2.4	CONCLUSIONS.....	43

3	MAGNETOVISCOSITY OF DILUTE SUSPENSIONS OF MAGNETIC ELLIPSOIDS IN CONSTANT MAGNETIC FIELDS	45
3.1	CALCULATION OF THE MAGNETOVISCOSITY OF THE SUSPENSION	49
3.2	SIMULATION PARAMETERS.....	53
3.3	RESULTS AND DISCUSSION	53
3.4	CONCLUSIONS.....	64
4	MAGNETOVISCOSITY OF DILUTE MAGNETIC FLUIDS IN OSCILLATING AND ROTATING MAGNETIC FIELDS.....	66
4.1	CALCULATION OF THE MAGNETOVISCOSITY OF THE SUSPENSION.....	70
4.2	SIMULATION PARAMETERS AND CONDITIONS	71
4.3	SIMULATION RESULTS AND DISCUSSION.....	72
4.4	CONCLUSIONS.....	85
	BIBLIOGRAPHY.....	87

LIST OF FIGURES

Figure 1-1: Schematic sketch of a magnetic particle in a ferrofluid.....	1
Figure 1-2: Magnetization curve for particles of 9 nm of cobalt ferrite in hexane.....	6
Figure 1-3: Brownian, Néel, and effective relaxation times at 298 K for magnetite nanoparticles suspended in water as a function of magnetic core radius.	10
Figure 1-4: Sketch of a magnetic particle under shear flow and magnetic field.	12
Figure 1-5: Particle model and coordinates axes.	14
Figure 1-6: TEM image from ferrofluids composed of spherical particles (left) and SEM image of a suspension composed of tri-axial ellipsoidal particles (right).	24
Figure 2-1: Type of ellipsoidal particles used in the simulations.	30
Figure 2-2: Dimensionless equilibrium magnetization as a function of Langevin parameter.....	32
Figure 2-3: Relaxation of dimensionless normalized magnetization for $\alpha = 0.1$	32
Figure 2-4: Variation of the magnetization with time when an external oscillating magnetic field is applied, for $\alpha = 0.1$ and $\tilde{\Omega} = 0.4$	34
Figure 2-5: Real (a) and imaginary (b) components of the dimensionless complex susceptibility as a function of dimensionless frequency.....	36
Figure 2-6: Real (a) and imaginary (b) components of the dimensionless complex susceptibility as a function of $\tilde{\Omega}\tilde{\tau}_{eff}/2$	37
Figure 2-7: Relaxation of dimensionless normalized magnetization for different values of Langevin parameter and comparison with Kalmykov and Titov's model.....	41

Figure 2-8: Real and imaginary components of the dimensionless complex susceptibility as a function of the dimensionless frequency for different probe field strengths..... 42

Figure 3-1: Intrinsic magnetoviscosity of a suspension of spherical particles as a function of Langevin parameter for different values of rotational Péclet number, and comparison with results from [47]. Inset, comparison with results from Brenner and Weissman (B & W) [52]..... 55

Figure 3-2: Intrinsic magnetoviscosity of a suspension of spherical particles as a function of rotational Péclet number for different values of Langevin parameter..... 57

Figure 3-3: Intrinsic magnetoviscosity of suspensions of ellipsoidal particles as a function of Langevin parameter for $Pe_r / K_{r,\min} = 5.0$.. 58

Figure 3-4: Intrinsic magnetoviscosity of suspensions of ellipsoidal particles as a function of rotational Péclet number for $\alpha = 3.0$. 59

Figure 3-5: Normalized intrinsic magnetoviscosity as a function of $Pe_{r,\text{eff}}$ for different values of α . 62

Figure 3-6: Orientational distribution of the magnetic dipole moment of (a) spherical particles, (b) prolate particles, (c) scalene1 particles, and (d) oblate particles, for $\alpha = 10$ and $Pe_{r,\text{eff}} = 18.93$.. 63

Figure 4-1: Experimental reduced viscosity $\eta_r = \eta^m / \eta$ versus magnetic field H for different frequencies f : \bullet : $f = 0$; \blacksquare : $f = 52$ Hz; \blacktriangle : $f = 150$ Hz; \blacklozenge : $f = 345$ Hz; $+$: $f = 645$ Hz; Δ : $f = 1480$ Hz. η is the viscosity of the suspension in zero magnetic field. 67

Figure 4-2: Torque required to rotate a spindle surrounded with ferrofluid at a rate of 100 rpm as function of applied field magnitude, rotation direction, and frequency..... 70

Figure 4-3: Dependence of the intrinsic magnetoviscosity on the magnitude and frequency of an oscillating magnetic field for $Pe_r = 0.1$.	73
Figure 4-4: Dependence of the intrinsic magnetoviscosity on the magnitude and frequency of (a) a co-rotating and (b) a counter-rotating magnetic field for $Pe_r = 0.1$.	74
Figure 4-5: Dependence of the intrinsic magnetoviscosity on the Péclet number and frequency of an oscillating magnetic field for $\alpha = 1$.	75
Figure 4-6: Dependence of the intrinsic magnetoviscosity on the Péclet number and frequency of (a) a co-rotating and (b) a counter-rotating magnetic field for $\alpha = 1$.	76
Figure 4-7: Minimum value of the intrinsic magnetoviscosity as a function of the Langevin parameter and Péclet number for (a) an oscillating and (b) a co-rotating magnetic field.	78
Figure 4-8: Normalized effective viscosity of the suspension as a function of the Langevin parameter for $Pe_r = 0.1$ and $\phi = 0.01$.	79
Figure 4-9: Time variation of the mean angular displacement of magnetic particles in both (a) co-rotating and (b) counter-rotating magnetic fields for $\alpha = 4$ and $Pe_r = 1$.	81
Figure 4-10: Comparison of variations of the mean angular displacement of magnetic particles in oscillating and co-rotating magnetic fields at $\tilde{\Omega} = 2.5$ for $\alpha = 1$ and $Pe_r = 1$.	83
Figure 4-11: Variation of the macroscopic magnetic torque in the flow vorticity direction (x -axis) with time in an oscillating and a co-rotating magnetic field at $\tilde{\Omega} = 2.5$ for $\alpha = 1$ and $Pe_r = 1$.	83

Figure 4-12: Intrinsic magnetoviscosity in co-rotating magnetic field as function of the angular slip velocity for $\alpha = 1$ and $Pe_r = 0.1$ 84

LIST OF TABLES

Table 2.1: Aspect ratios and rotational hydrodynamic resistance coefficients of the different types of particles used in the simulations. Here $\tilde{a}_1 = a_1/a_3$, $\tilde{a}_2 = a_2/a_3$, and

$\hat{K}_r = K_r/a_3^3$ 31

Table 2.2: Dimensionless effective relaxation time from simulations and theory for each type of particle 33

1 INTRODUCTION

1.1 Magnetic fluids

Magnetic fluids, commonly referred to as ferrofluids, are suspensions of permanently magnetized nanoparticles with diameter of order 5-15 nm suspended in a non-magnetic carrier liquid, usually water or oil, and volume concentration up to about 10%. These magnetic nanoparticles are typically single domain superparamagnetic particles of magnetite (Fe_3O_4), maghemite ($\gamma\text{-Fe}_2\text{O}_3$), various types of ferrites, iron, nickel, cobalt and other magnetic materials characterized by a magnetic dipole moment μ [1]. The magnetic nanoparticles are often coated with an organic surfactant to prevent agglomeration of particles due to both attractive van der Waals and magnetic forces (see Figure 1-1). Additionally, thermal agitation keeps the particles suspended because of Brownian motion, which results from constant and random collisions with molecules of the surrounding fluid.

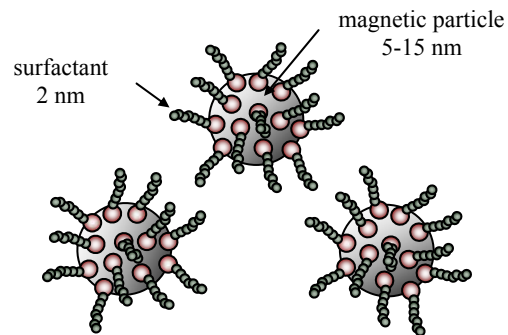


Figure 1-1: Sketch of magnetic particles in a ferrofluid

Since their invention in 1964, motivated by the objective of converting heat to work without mechanical parts [1], ferrofluids have been a challenging subject for fluid mechanics as well as for various applications [2]. Some of these applications are for example the cooling of loudspeakers with magnetic fluids, liquid O-rings in rotary and exclusion seals, inertial dampers in shock absorbers, or even in medicine for drug targeting, for magnetic hyperthermia in cancer treatment, or as bio-sensors [3, 4]. The use of magnetic fluids has attracted attention over the last decades because they exhibit functional properties, both magnetic and rheological, when they are subjected to an external magnetic field. Magnetic control of flow properties of these fluids results in several phenomena such as viscosity increases in constant magnetic fields [5, 6], the so-called “negative viscosity effect” in oscillating magnetic fields [7], and field induced flow in uniform rotating magnetic fields [8], leading to interesting consequences for hydrodynamics in general and for applications in science and engineering.

1.2 Magnetic properties of ferrofluids

Because of their small size, the suspended particles can be treated as magnetic dipoles in the carrier liquid. When a constant magnetic field \mathbf{H} is applied on a magnetic fluid it exerts a torque $\mathbf{T}_m = \mu_0(\boldsymbol{\mu} \times \mathbf{H})$ tending to align the magnetic dipole moment of the particles with the field, resulting in suspensions with superparamagnetic behavior. It means a high magnetization in low to moderate magnetic fields.

1.2.1 Equilibrium magnetization and Langevin function

The magnetization \mathbf{m} of a homogeneous magnetic fluid can be calculated from

$$\mathbf{m} = \frac{1}{V} \sum_{i=1}^N \boldsymbol{\mu}_i, \quad (1.1)$$

where V is the volume of the suspension and N is the number of particles. In dimensionless form, i.e., the magnetization divided by its saturation value, is then given as

$$\tilde{\mathbf{m}} = \frac{\mathbf{m}}{m_s} = \frac{1}{N\mu} \sum_{i=1}^N \boldsymbol{\mu}_i. \quad (1.2)$$

The latter expression represents the average dimensionless magnetization of a magnetic fluid. In this study the focus is on the magnetization in the direction of the applied field, and henceforth it will be assumed that the ferrofluid is a dilute system where there are not magnetic or hydrodynamic interactions between particles.

In the absence of an applied magnetic field, the particles are randomly oriented and the suspension does not have a net magnetization. When the suspension is subjected to an external magnetic field the magnetic dipole moments of the particles tend to align along the direction of the applied magnetic field either by particle rotation or by rotation of the dipole moment within the particle. However, for low field strengths this tendency is partially overcome by thermal agitation. As the magnetic field strength increases the magnetic dipole of the particles becomes increasingly aligned with the field direction until it achieves a saturation state where the dipoles are almost completely aligned with the magnetic field.

Considering a collection of single domain magnetic particles suspended in a non-magnetic carrier fluid, the magnitude of the torque on each particle exerted by an external magnetic field is given by:

$$T = \mu_0 \mu H \sin \theta, \quad (1.3)$$

where θ is the angle between $\boldsymbol{\mu}$ and \mathbf{H} . The energy necessary to turn the dipole to any angle θ is

$$W = \int_0^\theta T d\theta = \mu_0 \mu H (1 - \cos \theta), \quad (1.4)$$

where W is the work stored as potential energy to re-orient the dipole parallel to the field. Thermal agitation opposes this alignment, thus, Boltzmann statistics describes the number of dipoles having energy W as [1]

$$n_d(\theta, \phi) = \frac{N_d \alpha}{4\pi \sinh \alpha} e^{\alpha \cos \theta}, \quad (1.5)$$

where N_d is the total number of dipoles and $\alpha = (\mu_0 \mu H) / (k_B T)$, being k_B Boltzmann's constant, and T the absolute temperature. If particles with their dipoles forming an angle θ with the field are considered, integrating (1.5) over ϕ the following expression is obtained

$$n_d(\theta) = \frac{N_d \alpha}{2 \sinh \alpha} e^{\alpha \cos \theta}. \quad (1.6)$$

For what the effective magnetic dipole moment of a particle is its component along the field direction, i.e. $\mu \cos \theta$. Therefore, the average value of $\mu \cos \theta$ is given by

$$\langle \mu \cos \theta \rangle = \frac{\int_0^\pi \mu \cos \theta n_d(\theta) \sin \theta d\theta}{\int_0^\pi n_d(\theta) \sin \theta d\theta} = \mu \left(\coth \alpha - \frac{1}{\alpha} \right). \quad (1.7)$$

Let n be the number of particles in a unit volume of fluid, then, the magnetization m along the magnetic field direction of ferrofluid is $m = n \langle \mu \cos \theta \rangle$, and its saturation value m_s , in terms of the dipole of the particles, is $m_s = n\mu$. Therefore, from (1.7), the dimensionless magnetization of the suspension becomes

$$\tilde{m} = \frac{m}{m_s} = \coth \alpha - \frac{1}{\alpha} \equiv L(\alpha), \quad (1.8)$$

where $L(\alpha)$ denotes the *Langevin function*, and α is so-called the Langevin parameter.

Figure 1-2 shows an experimental magnetization curve for cobalt ferrite (CoFe_2O_4) nanoparticles suspended in hexane. The magnetization curve saturates at high values of α where the magnetic field dominates the Brownian torque resulting in particles with their

magnetic dipole moments almost aligned in the field direction. On the other hand, at low α , the rotational Brownian motion dominates and the particles have random orientations.

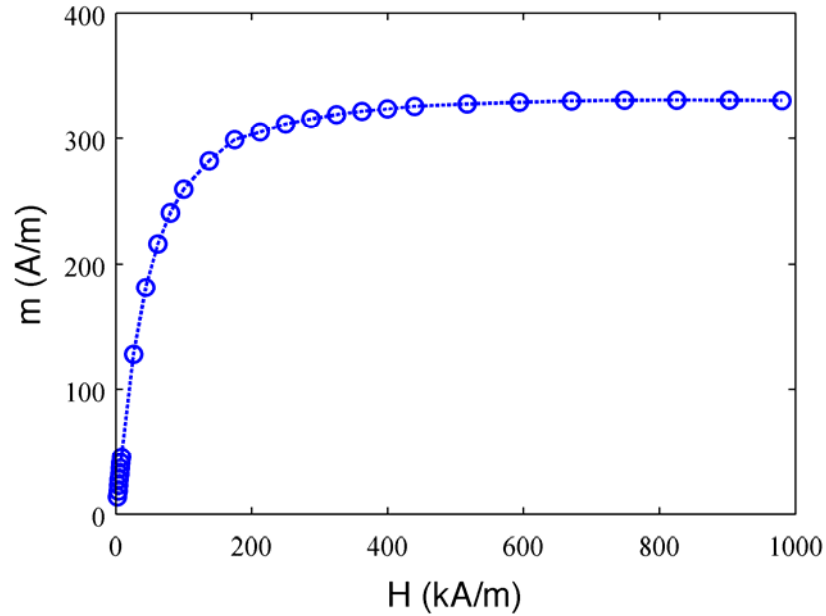


Figure 1-2: Magnetization curve for particles of 9 nm of cobalt ferrite in hexane. Volume fraction is 0.1%.

1.2.2 Dynamic magnetization and Debye model

There are two mechanisms by which the particle's magnetic dipole moment can be aligned along the field direction in a ferrofluid: Brownian relaxation and Néel relaxation [1]. Brownian relaxation occurs if the magnetic moment of the particle is fixed in its crystal structure [2]. The relaxation of this kind of particles implies rotation of the whole particle and is characterized by a Brownian relaxation time of hydrodynamic origin. In order to obtain a model for this relaxation mode of the magnetization, it is necessary to solve the Smoluchowski equation for the orientational distribution function $f(\theta, \phi, t)$ of the magnetic dipole moments, which in vectorial form is written as [9]

$$\frac{\partial f}{\partial t} = \nabla_{\Phi} \cdot (\mathbf{D}_r \cdot \nabla_{\Phi} f) - \nabla_{\Phi} \cdot (\mathbf{T}_m \cdot \zeta_r^{-1}) f. \quad (1.9)$$

In (1.9) ∇_{Φ} is the differential operator in orientation space, \mathbf{D}_r is the rotational diffusion tensor given by the generalized Stokes-Einstein equation as $\mathbf{D}_r = (k_B T) \zeta_r^{-1}$, and ζ_r is the rotational hydrodynamic resistance dyadic. We are only interested in solutions that are dependent on the zenithal angle θ (see Figure 1-5) because it alone enters into the potential energy of the permanent dipole in the external field, as shown in Section 1.2.1. For the particular case of isotropic particles, the rotational hydrodynamic resistance is expressed by the scalar ζ_r . Thus, for a constant magnetic field $\mathbf{H} = H_0 \mathbf{i}_z$, (1.9) would be written as

$$\frac{\zeta_r}{k_B T} \frac{\partial f}{\partial t} = \frac{1}{\sin \theta} \frac{\partial}{\partial \theta} \left(\sin \theta \frac{\partial f}{\partial \theta} \right) + \frac{\mu_0 (\mu H_0)}{k_B T} \frac{1}{\sin \theta} \frac{\partial}{\partial \theta} (\sin^2 \theta f). \quad (1.10)$$

Solving (1.10) for values of $(\mu_0 \mu H)/(k_B T) \ll 1$, the expression for the mean dipole of the system, $\langle \mu \cos \theta \rangle = \int \mu \cos \theta f \sin \theta d\theta$, is used to obtain the dimensionless magnetization of the suspension $\tilde{m}_z(t) = \langle \mu \cos \theta \rangle / \mu$. Two special situations are readily obtained: (i) relaxation upon switching off the field, and (ii) response to an oscillating field. In the first case, we assume that the system is at equilibrium with an external magnetic field at $t = 0$, and suddenly the field is turned off, $H_0 = 0$, for $t > 0$. At $t = 0$ the distribution function is given by (1.6)

$$f(t=0) = \frac{\alpha}{2 \sinh \alpha} e^{\alpha \cos \theta}, \quad (1.11)$$

where (1.11) can be expanded to first order in the small Langevin parameter as

$$f(t=0) = \frac{\alpha}{2\alpha} \left[1 + \alpha \cos \theta + O(\alpha^2) \right] = \frac{1}{2} \left(1 + \frac{\mu_0 \mu \cos \theta}{k_B T} \right). \quad (1.12)$$

This suggests an orientation distribution function in (1.10) of the form

$$f = \frac{1}{2} \left(1 + \frac{\mu_0 \mu \cos \theta}{k_B T} g(t) \right). \quad (1.13)$$

Since $H_0 = 0$ for $t > 0$, and substituting (1.13) in (1.10) we obtain that $g = e^{-t/\tau}$, where $\tau = \zeta_r / (2k_B T)$ is called the Debye (or Brownian, τ_B) relaxation time. This result for the function g is then used to obtain the dimensionless magnetization, along the magnetic field direction, of the suspension

$$\tilde{m}_z = \frac{1}{3} \alpha \exp(-t/\tau_B) \quad (1.14)$$

In the case of a weak external oscillating magnetic field, $\mathbf{H} = H_0 \cos(\Omega t) \mathbf{i}_z$, the dipole moment of the particles follows the oscillations of the magnetic field with a phase-

lag between the field and the particles. The z -component of the dimensionless magnetization is then

$$\tilde{m}_z = \left(\frac{1}{3}\alpha\right) \text{Re}\{\hat{\chi}e^{j\Omega t}\} = \left(\frac{1}{3}\alpha\right) [\tilde{\chi}'\cos(\Omega t) + \tilde{\chi}''\sin(\Omega t)]. \quad (1.15)$$

where $\hat{\chi} = \tilde{\chi}' - j\tilde{\chi}''$ is the dimensionless complex susceptibility. The nondimensional in-phase and out-of-phase susceptibilities, $\tilde{\chi}'$ and $\tilde{\chi}''$ respectively, are frequency-dependent

$$\tilde{\chi}' = \frac{1}{1+(\Omega\tau)^2}, \quad \tilde{\chi}'' = \frac{(\Omega\tau)}{1+(\Omega\tau)^2}. \quad (1.16)$$

Experimental techniques to measure relaxation time of magnetization have been developed by Fannin [10-12], consisting in the determination of the complex susceptibility when an alternating magnetic field is applied.

On the other hand, under certain conditions the magnetic moment may rotate inside the particle; thus, in Néel relaxation, the magnetic moment aligns without physical rotation of the particle. This kind of relaxation takes place if the thermal energy overcomes the energy barrier provided by the magnetocrystalline anisotropy of the magnetic material. The Néel relaxation time is given by

$$\tau_N = \tau_0 \exp\left(\frac{KV_c}{k_B T}\right), \quad (1.17)$$

where τ_0 is a decay time between 10^{-10} to 10^{-8} sec. [12], K is the magnetocrystalline anisotropy constant, and V_c is the volume of the magnetic core of the particle.

It is important to note that both relaxation mechanisms are particle size dependent, and thus, for a monodisperse suspension, the effective magnetic relaxation time τ will follow the shorter process, as seen from [13]

$$\tau = \frac{\tau_B \tau_N}{\tau_B + \tau_N} . \quad (1.18)$$

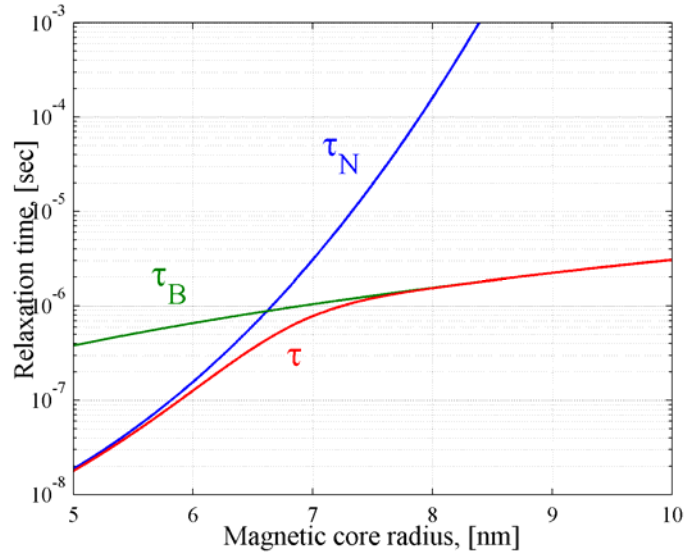


Figure 1-3: Brownian, Néel, and effective relaxation times at 298 K for magnetite nanoparticles suspended in water as a function of magnetic core radius.

As shown in Figure 1-3, the transition from Néel to Brownian relaxation time may be considered to take place for particles with a size d_s obtained by equating τ_B and τ_N ; thus, $d_s = 8.5$ nm for iron and 4 nm for cobalt [1].

In this work we consider monodisperse suspensions composed of magnetic nanoparticles that relax following the Brownian relaxation mechanism, therefore equations (1.8), and (1.14) to (1.16) form the basis to analyze magnetic properties of the suspension.

1.3 Rheological properties

The presence of suspended particles in a fluid changes the effective rheological properties of the suspension, especially its viscosity. The first theoretical treatment of such changes in the viscosity for dilute suspensions of spherical particles was given by Einstein, who obtained the following relation for the viscosity of a force and torque free suspension [14]

$$\frac{\eta}{\eta_0} = 1 + \frac{5}{2}\phi. \quad (1.19)$$

This can be expressed more generally as [15]

$$\frac{\eta}{\eta_0} = 1 + C_1\phi + C_2\phi^2 + O(\phi^3). \quad (1.20)$$

Here η_0 is the viscosity of the carrier fluid, and the coefficient C_2 reflects interactions between pairs of spheres, influenced by the spatial distribution of the particles.

In the case of a magnetic fluid in a simple shear flow field, if an external magnetic field is applied the particles will rotate relative to the fluid resulting in an additional

change in the viscosity of the suspension. As an example, consider the spherical particle shown in Figure 1-4 possessing a permanent particle-locked magnetic dipole moment. In the absence of an external magnetic field the suspended particle rotates freely with its axis of rotation parallel to the flow vorticity \mathbf{w} . When a constant (i.e. stationary) magnetic field is applied and assuming that the field is perpendicular to the vorticity of the flow, the magnetic torque exerted on the particle counteracts the hydrodynamic torque, aligning the dipole moment with the field. The counteraction of the torques results in hindered rotation of the particles, thus increasing the rate of mechanical energy dissipation, and hence the effective viscosity of the suspension [16]. In the case where the magnetic field is collinear with the vorticity, the particle can rotate freely and no field influence on the viscosity of the suspension will be observed.

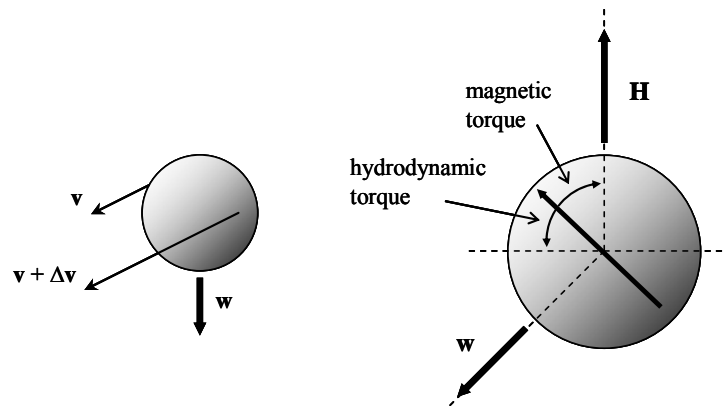


Figure 1-4: Sketch of a magnetic particle under shear flow and magnetic field.

On the other hand, if an oscillating magnetic field with frequency higher than the local angular velocity of the fluid is applied, the torque acting on each particle causes the particles to rotate faster than the fluid, reducing the friction between adjacent fluid layers,

thus decreasing the effective viscosity of the suspension. Therefore, at high frequencies of the magnetic field, the part of the field-dependent viscosity can become negative, a phenomenon known as “the negative viscosity effect”, which was first observed by Bacri *et al.* [7] and theoretically described by Shliomis and Morozov [17].

It is interesting to note that the viscosity appears to be anisotropic depending not only on the strength but also on the direction of the field relative to the flow [2]. Moreover, owing to the presence of internal couples in the suspension, the bulk stress tensor for suspensions of dipolar particles subjected to an external magnetic field becomes asymmetric [6,9,10].

1.4 Rotational Brownian motion of an orthotropic particle in magnetic and shear fields

For a tri-axial ellipsoidal particle (an orthotropic particle¹), physical and magnetic properties are most naturally written in a cartesian coordinate system with axes aligned with the principal semi-axes of the ellipsoid (primed axes) rather than relative to the coordinate axes of the laboratory space (unprimed axes), as illustrated in Figure 1-5. An ellipsoid has three principal semi-axes a_1 , a_2 , and a_3 , directed along the x' , y' , and z' -axis, respectively. In the present work the following cases will be considered: spherical particles $a_1 = a_2 = a_3$; prolate ellipsoids $(a_1 = a_2) < a_3$; oblate ellipsoids $a_1 < (a_2 = a_3)$; and scalene ellipsoids $a_1 \neq a_2 \neq a_3$.

¹ An orthotropic particle has three planes of symmetry through its centre of volume.

It is further considered that the magnetic dipole moment of the particle, $\boldsymbol{\mu}'$, is directed along the z' -axis, which may not necessarily be the major semiaxis of the particle. The magnetic field, \mathbf{H} , is assumed to be applied in the yz -plane and the simple shear flow is along the y -axis.

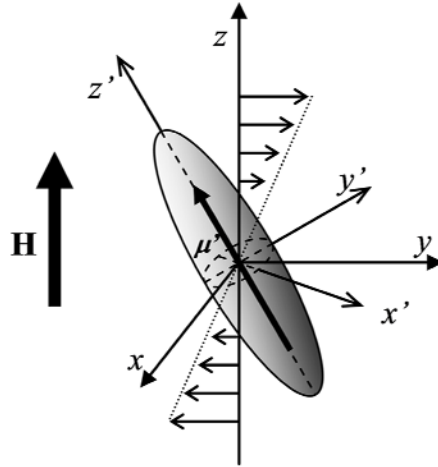


Figure 1-5: Particle model and coordinates axes.

If the shear rate is denoted by $\dot{\gamma}$, then the unperturbed flow velocity \mathbf{v} , the local angular velocity of the fluid $\boldsymbol{\omega}_f$, and the rate-of-strain tensor $\boldsymbol{\Gamma}$ are given by

$$\mathbf{v} = \dot{\gamma} z \mathbf{i}_y, \quad \boldsymbol{\omega}_f = -\frac{1}{2} \dot{\gamma} \mathbf{i}_x, \quad \boldsymbol{\Gamma} = \frac{1}{2} \dot{\gamma} (\mathbf{i}_y \mathbf{i}_z + \mathbf{i}_z \mathbf{i}_y). \quad (1.21)$$

The rotational motion of a particle is described by classical mechanics as

$$\boldsymbol{\omega} dt = d\boldsymbol{\Phi}, \quad I \frac{d\boldsymbol{\omega}}{dt} = \sum \mathbf{T}, \quad (1.22)$$

where $\boldsymbol{\omega}$ is the angular velocity of the particle, $d\boldsymbol{\Phi}$ is the infinitesimal rotation vector, I the inertia moment, and \mathbf{T} the torques acting on the particle.

Brownian dynamics simulations are based on the integration of the stochastic angular momentum equation in order to obtain the time evolution of the particle orientation. Because of the small sizes and low mass of nanoparticles in a ferrofluid, the moment of inertia of the particle is negligible. Therefore, the time scale $I/\zeta_r \sim 10^{-11}$ s for the angular velocity correlation is short compared to the natural observation time for Brownian motion $\sim 10^{-6}$ s, which implies that the angular velocity quickly approaches the Maxwell-Boltzmann distribution [18], and whence the inertial term in the equation of motion can be neglected.

There are three kinds of torque acting on the particle: hydrodynamic torque \mathbf{T}_h , magnetic torque \mathbf{T}_m , and Brownian torque \mathbf{T}_B . In the inertialess limit the angular momentum balance is given as

$$\mathbf{T}'_h + \mathbf{T}'_m + \mathbf{T}'_B = \mathbf{0} \quad (1.23)$$

where the prime denotes a vector relative to body-fixed axes.

For the hydrodynamic torque, it is well known that at low Reynolds number the force on a rigid particle of arbitrary shape is directly proportional to both the fluid viscosity and the free stream velocity. If it is assumed that the rigid particle is immersed in a shear flow and that the quasistatic Stokes equation is applicable, then

$$\nabla^2 \mathbf{v} = \frac{1}{\eta_0} \nabla p \quad (1.24)$$

$$\nabla \cdot \mathbf{v} = 0, \quad (1.25)$$

with boundary conditions given by

$$\mathbf{v} = \mathbf{U}_0 + \boldsymbol{\omega} \times \mathbf{r}_0 \text{ on particle surface,} \quad (1.26)$$

$$\mathbf{v} \rightarrow \mathbf{u}_0 + \boldsymbol{\omega}_f \times \mathbf{r}_0 + \boldsymbol{\Gamma} \cdot \mathbf{r}_0 \text{ as } r \rightarrow \infty, \quad (1.27)$$

where 0 denotes any point in the particle, \mathbf{U}_0 the velocity of this point, \mathbf{r}_0 the position vector of a point relative to 0, and \mathbf{u}_0 the velocity of the undisturbed flow at 0. Equation (1.27) corresponds to a decomposition of the original shearing motion into translational, rotational and pure shear contributions.

Owing to the linearity of the equations of motion and boundary conditions it is possible to establish and solve separate problems satisfying (1.26) and (1.27), with which the hydrodynamic torque exerted by the fluid on the particle by virtue of the individual rotational motion and pure shear is given by [19, 20]

$$\mathbf{T}'_h = -\eta_0 \left[\mathbf{K}'_r \cdot (\boldsymbol{\omega}' - \boldsymbol{\omega}'_f) + \boldsymbol{\tau}'_0 : \boldsymbol{\Gamma}' \right] \quad (1.28)$$

where \mathbf{K}'_r is the hydrodynamic resistance dyadic, $\boldsymbol{\omega}'$ and $\boldsymbol{\omega}'_f$ are the angular velocity of both the particle and the fluid respectively, $\boldsymbol{\Gamma}'$ is the rate-of-strain tensor relative to

body-fixed axes, and $\boldsymbol{\tau}'_0$ is a constant triadic dependent only upon the shape of the particle.

Defining

$$\varepsilon_j = \int_0^\infty \frac{d\lambda}{(a_j + \lambda)\Delta(\lambda)} \quad (j=1,2,3) \quad (1.29)$$

in which

$$\Delta(\lambda) = \left[(a_1^2 + \lambda)(a_2^2 + \lambda)(a_3^2 + \lambda) \right]^{1/2}, \quad (1.30)$$

the polyadics in (1.28), for an orthotropic particle, have the form [20]

$$\mathbf{K}'_r = \frac{16\pi}{3} \left[\frac{a_2^2 + a_3^2}{a_2^2 \varepsilon_2 + a_3^2 \varepsilon_3} \mathbf{i}_x \mathbf{i}_x + \frac{a_3^2 + a_1^2}{a_3^2 \varepsilon_3 + a_1^2 \varepsilon_1} \mathbf{i}_y \mathbf{i}_y + \frac{a_1^2 + a_2^2}{a_1^2 \varepsilon_1 + a_2^2 \varepsilon_2} \mathbf{i}_z \mathbf{i}_z \right], \quad (1.31)$$

$$\begin{aligned} \boldsymbol{\tau}'_0 = \frac{8\pi}{3} & \left[\frac{a_3^2 - a_2^2}{a_3^2 \varepsilon_3 + a_2^2 \varepsilon_2} (\mathbf{i}_x \mathbf{i}_y \mathbf{i}_z + \mathbf{i}_x \mathbf{i}_z \mathbf{i}_y) + \frac{a_1^2 - a_3^2}{a_1^2 \varepsilon_1 + a_3^2 \varepsilon_3} (\mathbf{i}_y \mathbf{i}_z \mathbf{i}_x + \mathbf{i}_y \mathbf{i}_x \mathbf{i}_z) \right. \\ & \left. + \frac{a_2^2 - a_1^2}{a_2^2 \varepsilon_2 + a_1^2 \varepsilon_1} (\mathbf{i}_z \mathbf{i}_x \mathbf{i}_y + \mathbf{i}_z \mathbf{i}_y \mathbf{i}_x) \right]. \end{aligned} \quad (1.32)$$

On the other hand, the magnetic torque on a particle in a magnetic field can be obtained by integrating the Maxwell stress tensor over the surface of the particle S_p [21]

$$\mathbf{T}_m = \oint_{S_p} \mathbf{r} \times \left[d\mathbf{S} \cdot \left(\mathbf{B}\mathbf{H} - \frac{1}{2} \mu_e H^2 \mathbf{I} \right) \right], \quad (1.33)$$

where \mathbf{r} is the position vector, \mathbf{B} the magnetic flux density, and \mathbf{H} the magnetic field. For the case of a magnetized spherical particle in a uniform magnetic field the solution is well known [21].

Despite the geometry of the particle and since each particle in the ferrofluid is considered as a permanently magnetized nanoparticle, they can be modeled as infinitesimal dipoles where the magnetic torque would be given by

$$\mathbf{T}'_m = \mu_0 (\boldsymbol{\mu}' \times \mathbf{H}'), \quad (1.34)$$

where $\mathbf{H}' = \mathbf{A} \cdot \mathbf{H}$ is the magnetic field transformed to the body-fixed axes through the transformation matrix \mathbf{A} . The transformation matrix is an operator that, acting on the components of a vector in a coordinate system, yields the components of the vector in other coordinate system [22]. Because only three coordinates are necessary to specify any orientation of a rigid body, the Euler angles have been the most common set of coordinates to form proper orthogonal transformation matrices. However, the Euler angles are difficult to use in numerical solutions because the trigonometric functions involved could lead to a singular problem.

In order to free the algorithm from singularities the transformation matrix is then expressed in terms of the Euler parameters, e_0 , e_1 , e_2 , and e_3 , as [22]

$$\mathbf{A} = \begin{bmatrix} e_0^2 + e_1^2 - e_2^2 - e_3^2 & 2(e_1e_2 + e_0e_3) & 2(e_1e_3 - e_0e_2) \\ 2(e_1e_2 - e_0e_3) & e_0^2 - e_1^2 + e_2^2 - e_3^2 & 2(e_2e_3 + e_0e_1) \\ 2(e_1e_3 + e_0e_2) & 2(e_2e_3 - e_0e_1) & e_0^2 - e_1^2 - e_2^2 + e_3^2 \end{bmatrix} \quad (1.35)$$

in which the Euler parameters satisfy the relation $e_0^2 + e_1^2 + e_2^2 + e_3^2 = 1$.

Substituting (1.28) and (1.34) into (1.23), and solving for $\boldsymbol{\omega}'$, we obtain

$$\boldsymbol{\omega}' = \boldsymbol{\omega}'_f - (\mathbf{K}'_r)^{-1} \cdot (\boldsymbol{\tau}'_0 : \boldsymbol{\Gamma}') + (\eta_0 \mathbf{K}'_r)^{-1} \cdot (\mu_0 \boldsymbol{\mu}' \times \mathbf{H}') + (\eta_0 \mathbf{K}'_r)^{-1} \cdot \mathbf{T}'_B \quad (1.36)$$

In order to reduce the number of variables and parameters, (1.38) can be expressed in dimensionless form using appropriate scaled variables. There are two time scales to consider: (i) a diffusive time scale, $1/D_r$, and (ii) a convective time scale, $1/\dot{\gamma}$. The diffusive time scale is the time required for particle rotation due to Brownian torques, whereas the convective time scale is associated with rotation due to the local vorticity of the flow. Because the Brownian torque results from collisions between the particle and the fluid molecules it is natural to assume that the diffusive time scale is shorter than the time scale in which we observe the rotation of the particle. Therefore, to capture the faster process of the particle in the simulations, a diffusive time scale given by $1/D_{r,\max}$ is used to nondimensionalize the angular velocity of the particle. Hence, the dimensionless variables are then defined as

$$\tilde{\boldsymbol{\omega}}' = \frac{\boldsymbol{\omega}'}{D_{r,\max}}, \quad \tilde{\boldsymbol{\omega}}'_f = \frac{\boldsymbol{\omega}'_f}{\dot{\gamma}}, \quad \tilde{\mathbf{K}}'_r = \frac{\mathbf{K}'_r}{K_{r,\min}}, \quad \tilde{\boldsymbol{\tau}}'_0 = \frac{\boldsymbol{\tau}'_0}{K_{r,\min}},$$

$$\tilde{\Gamma}' = \frac{\Gamma'}{\dot{\gamma}}, \quad \tilde{\mu}' = \frac{\mu'}{\mu}, \quad \tilde{\mathbf{H}}' = \frac{\mathbf{H}'}{H}. \quad (1.37)$$

In (1.37), μ and H are the magnitudes of $\boldsymbol{\mu}'$ and \mathbf{H}' respectively, and $D_{r,\max}$ is the larger of the diagonal terms in the rotational diffusion tensor \mathbf{D}'_r , written relative to particle-fixed axes. The rotational diffusion tensor is given by the generalized Stokes-Einstein equation $\mathbf{D}'_r = k_B T (\eta_0 \mathbf{K}'_r)^{-1}$.

With these definitions in (1.36), setting $d\tilde{\boldsymbol{\Phi}}' = \tilde{\boldsymbol{\omega}}' d\tilde{t}$, where $d\tilde{\boldsymbol{\Phi}}'$ is the infinitesimal rotation vector, and finally integrating from time t to time $t + \Delta t$ using a first-order forward Euler method, which gives good numerical results when the diffusion coefficient is constant [18], and applying the fluctuation-dissipation theorem [18, 23] to the Brownian term, it is obtained

$$\Delta\tilde{\boldsymbol{\Phi}}' = \text{Pe}_r \left[\tilde{\boldsymbol{\omega}}'_f - (\tilde{\mathbf{K}}'_r)^{-1} \cdot (\tilde{\boldsymbol{\tau}}'_0 : \tilde{\Gamma}') \right] \Delta\tilde{t} + \alpha \left[(\tilde{\mathbf{K}}'_r)^{-1} \cdot (\tilde{\boldsymbol{\mu}}' \times \tilde{\mathbf{H}}') \right] \Delta\tilde{t} + \tilde{\mathbf{B}}' \cdot \tilde{\mathbf{w}}', \quad (1.38)$$

where $\text{Pe}_r = \dot{\gamma} / D_{r,\max}$ is the rotational Péclet number. The fluctuation-dissipation theorem relates short-time correlations of dynamical variables to dissipation constants such as $\mathbf{B}' \cdot \mathbf{B}'^T = 2k_B T (\eta_0 \mathbf{K}'_r)^{-1}$, where k_B is Boltzmann's constant, T the absolute temperature, and the superscript T implies transposition. Vector \mathbf{w} is a random vector characterized by a Gaussian distribution with zero mean, $\langle \mathbf{w} \rangle = 0$, and variance $\langle \mathbf{w} \cdot \mathbf{w} \rangle = \Delta t$. In (1.38)

$$\tilde{\mathbf{B}}' = \mathbf{B}' / (D_{r,\max})^{1/2} \quad \text{and} \quad \tilde{\mathbf{w}}' = \mathbf{w}' (D_{r,\max})^{1/2}$$

The algorithm proceeds from a starting configuration by calculating the change in orientation at each time step by evaluating (1.38) and using the relation between the angular velocity vector and the Euler parameters

$$\begin{bmatrix} \Delta e_0 \\ \Delta e_1 \\ \Delta e_2 \\ \Delta e_3 \end{bmatrix} = \frac{1}{2} \begin{bmatrix} e_0 & -e_1 & -e_2 & -e_3 \\ e_1 & e_0 & -e_3 & e_2 \\ e_2 & e_3 & e_0 & -e_1 \\ e_3 & -e_2 & e_1 & e_0 \end{bmatrix} \begin{bmatrix} 0 \\ \Delta \Phi'_x \\ \Delta \Phi'_y \\ \Delta \Phi'_z \end{bmatrix} \quad (1.39)$$

to evaluate the change in Euler parameters. The Euler parameters of each particle are renormalized after each time step.

1.5 Motivation

Commonly, ferrofluids are composed of spherical permanently magnetized nanoparticles suspended in water or an organic solvent (Figure 1-6). In order to describe the behavior of ferrofluids under certain conditions of external magnetic and flow fields several theories have been developed such as the Langevin function, to determine the equilibrium magnetization of the suspension, Debye's model, for the dynamic magnetization of a suspension of spherical particles, and equations for the magnetoviscosity, also for suspensions of spherical particles, solving the system of ferrohydrodynamic equations. Nevertheless, other type of particles such as fibers, rods, spheroids, plates, and their aggregating clusters have been studied due to their applicability in many different fields of modern technology. The paint, ceramic, and pharmaceutical industries use suspensions of anisotropic particles, the dynamics of which

differ significantly from systems composed of spherical particles [24]. The macroscopic properties of such suspensions – thermal conductivity, viscosity, magnetization, etc – greatly depend on the orientation of the particles in the medium. Thus, for example, the scattering and absorption properties of particles are affected by deviations of the particle morphology from that of a perfect sphere [25], the combined anisotropic morphology and directional interactions of magnetic peanut-shaped particles make them interesting candidates for the assembly of colloidal analogues of molecular crystals [26], and spheroids and rod-like particles are used to develop high-quality magnetic recording materials where the orientational distribution of the particles is carefully controlled by applied magnetic and flow fields [27]. These types of particles have been modeled as axisymmetric particles with two characteristic relaxation times, parallel and perpendicular to the symmetry axis, making feasible analytical solutions or numerical approximations, even considering interacting particles.

In the case of axisymmetric particles, some theoretical models have been developed by solving the Fokker-Planck equation for dilute suspensions [28-30]. The instantaneous orientation of a single axisymmetric particle is typically specified by a unit vector \mathbf{e} locked into the particle and lying along its symmetry axis, which typically coincides with the magnetic dipole. For this case, numerical solutions for the orientational distribution function $f(\mathbf{e})$ have also been obtained. For semi-concentrated suspensions, interactions between particles make necessary a numerical solution for the probability distribution function, which describes the average orientations of particles in the bulk of the suspension, or from the stochastic Langevin equation [23, 31-33].

All of the work discussed above considered suspensions of spheres or solids of revolution, such as spheroids and rods. However, the nanoparticles obtained in magnetic fluid synthesis are not perfectly spherical or axisymmetric. Moreover, in the use of ferrofluids as bio-sensors, purification fluids or drug delivery carriers, once the particles attach to an analyte or target, the particle loses its symmetry and the models developed are not able to describe the behavior of these suspensions. On the other hand, lithographic techniques may provide a method to produce asymmetric magnetic particles by design. This underscores the need to understand the dynamics of asymmetric magnetic particles, the orientation of which is not wholly specified by a simple unit vector locked into each particle.

The study of suspensions composed of tri-axial ellipsoidal particles (Figure 1-6) by numerical simulations, will allow us to understand the behavior of suspensions composed of asymmetric top particles where their orientations are characterized by three independent parameters, such as for example the Euler's angles, and furthermore three relaxation times, making more complex their study from an analytical and numerical point of view [9], especially in situations for which there is flow. Thus, alternative methods of simulation, suitable to tri-axial ellipsoids, are needed to study and model these types of suspensions.

The purpose of this work is to present simulations of rotational Brownian dynamics for magnetization and magnetoviscosity of a magnetic fluid composed of spherical or tri-axial ellipsoidal particles suspended in a Newtonian fluid and which is subjected to magnetic and shear flow fields. To do this a FORTRAN-95 code was implemented in

order to perform the simulations under diverse conditions of the external fields and different aspect ratios of the particles.

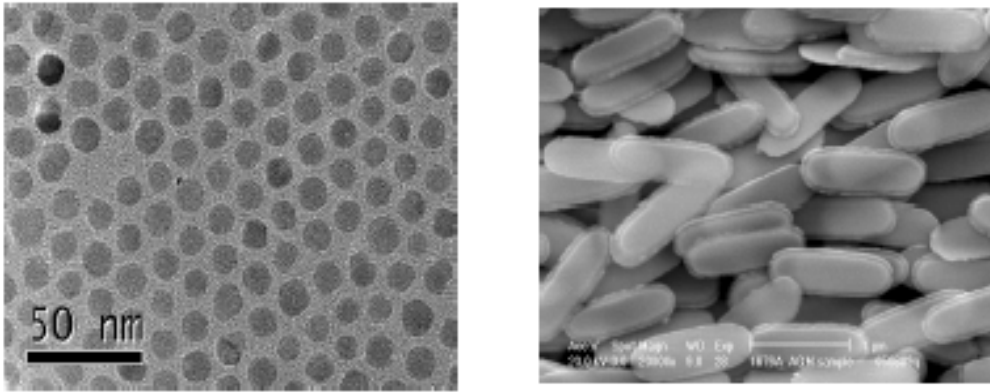


Figure 1-6: TEM image from ferrofluids composed of spherical particles (left) and SEM image of a suspension composed of tri-axial ellipsoidal particles (right).

2 ROTATIONAL BROWNIAN DYNAMICS SIMULATIONS OF NON-INTERACTING MAGNETIZED ELLIPSOIDS IN CONSTANT AND OSCILLATING MAGNETIC FIELDS

As mentioned in the previous chapter, magnetic fluids are composed usually of spherical magnetic nanoparticles and analytical models have been developed in order to describe the magnetization of dilute suspensions of these particles. In the case of concentrated systems, interparticle interactions become relevant and a numerical approach is typically required. Indeed, numerical solutions of the Langevin equations have been obtained and several methods for simulating the Brownian dynamics of spherical particles have been developed, such as the work by Ermak and McCammon [31], who considered hydrodynamic interactions between spherical particles, and Dickinson [23], who incorporated the effects of rotation-translation coupling. Their results show values of the translational diffusion coefficient and the rotational decay rate that are in good agreement with the theoretical values from the Oseen and Rotne-Prager diffusion tensors. More recently, Meriguet *et al.* [32] simulated the influence of an effective pair-interaction potential between spherical particles on the magnetization relaxation of ferrofluids through integration of the stochastic translational and rotational Langevin equations. They found that the relaxation time increases as the volume fraction of particles increases.

On the other hand, in the case of axisymmetric particles, the Brownian motion of ellipsoids in suspensions without external forces has been recently studied experimentally by Han *et al.* [34]. The experiments were restricted to two dimensions (2D) and the suspensions were made very dilute in order to avoid interactions between particles. In their work it was evident that a particle with a given initial angle will diffuse more rapidly along its long axis than along its short axis if the diffusion time is lower than the rotational relaxation time, τ_θ (anisotropic diffusion). As time progresses, memory of the initial orientation is lost, and diffusion becomes isotropic. More recently, direct visualization of dynamics of colloidal rods was carried out by Mukhija and Solomon [24]. They reported a particle tracking confocal microscopy method to characterize the translational and orientational dynamics of anisotropic particles undergoing Brownian motion in three dimensions. Their results showed that translational and rotational diffusion coefficients agree well with theory for prolate shaped particles in a dilute suspension.

Simulations have also been used to study the effects of an external force field on suspensions of nonspherical particles. An approach for modeling the rotational dynamics of axially symmetric magnetic particles in fluid suspensions, in the dilute limit, was developed by Scherer and Matutis [35]. Based on a generalized Lagrangian formulation for the equation of motion, they showed the effect of particle inertia on the susceptibility, suggesting that the peak of the imaginary part of the complex susceptibility shifts to higher frequencies as the moment of inertia increases.

In the case of asymmetric top particles, despite the difficulty in obtaining analytical solutions, an analytical model was obtained by Perrin [36] and Coffey *et al.* [37] for the

dynamics of a collection of non-interacting asymmetric-top particles in the cases of relaxation from an equilibrium field and response to an oscillating field, both in the limit of small applied fields. Perrin's solution was obtained by solving for the orientational distribution function, finding that the time-dependent polarization is given by three exponentials with distinct relaxation times. Additionally, fluorescence depolarization methods have been also used to investigate the rotational motion of molecules [38, 39] despite their hydrodynamic shape. This technique is based on the fact that when a chromophore rigidly bound to a macromolecule is excited by a light pulse, the anisotropy of fluorescence decays due to the Brownian rotation of the macromolecule [40]. Thus, Weber [41] obtained analytically that even for a molecule of irregular shape moving in a medium in which the resistance to the rotational motion is anisotropic, after an instantaneous light pulse, a polarized component of the fluorescence will show a maximum of three exponential decays. The same result was found later by Small and Isenberg [40] considering a general ellipsoid as a hydrodynamic model for a rigid body. Nevertheless, Chuang and Eisinger [42], and Erhenberg and Rigler [43] showed that for a general particle with the absorption vector along an arbitrary direction in the molecular frame, the time-dependent fluorescence depolarization caused by anisotropic rotation diffusion has a maximum of five exponential decays.

More recently, Kalmykov and Titov [44, 45] obtained analogous results to those of Perrin by averaging the non-inertial Langevin equation for rotational Brownian motion, considering the nonlinear transient response of non-interacting asymmetric tops to arbitrary fields and susceptibility to small probe fields in the presence of large bias fields. This approach yields an infinite hierarchy of differential-recurrence relations for the

statistical moments describing the orientational relaxation of particles, where the resulting system of moment equations is solved by a complex mathematical method known as the matrix continued fraction method. Their results show that the dipole relaxation function can be approximated, in the time domain, by three exponentials with distinct relaxation times and, the dynamic susceptibility, in frequency domain, by three Lorentzians.

The models obtained by Perrin and Kalmykov and Titov may be applied to the interpretation of experimental data on linear and non-linear response of dilute suspensions of magnetic nanoparticles of arbitrary shape, however these theories would benefit from verification. As proposed by Kalmykov and Titov, the models could be compared with results obtained through numerical simulations, because in computer simulations it is easier to achieve large values of the magnetic field. Therefore, the purpose of this chapter is to present simulation results for the rotational Brownian dynamics of non-interacting tri-axial ellipsoidal particles with an embedded magnetic dipole in order to validate the theory mentioned above, and show if it is applicable to the interpretation of experimental data. It is assumed that the magnetic dipole is rigidly locked into the particle, neglecting the effect of Néel relaxation.

2.1 Calculation of the magnetization of the suspension

To calculate the time evolution of the magnetization by numerical simulation it is necessary to express (1.2) in terms of the Euler parameters of the particles. Using the transformation matrix \mathbf{A} , the magnetization of the suspension can be obtained from

$$\tilde{m}_z = \frac{1}{n} \sum_{i=1}^n (e_0^2 - e_1^2 - e_2^2 + e_3^2)_i. \quad (2.1)$$

Thus, from (2.1) in conjunction with (1.38) and (1.39) making $Pe_r = 0$, the evolution with time of the magnetization can be obtained.

2.2 Magnetization response to weak magnetic fields

According to Perrin's analysis [36, 37] for the case of an ellipsoid with its magnetic dipole along one of its principal axes, say the z' -axis, Eqs. (1.14) and (1.15) continue to apply insofar as the relaxation time τ is replaced by an effective relaxation time, that in dimensionless form is given by

$$\tilde{\tau}_{eff} = \frac{2D_{r,max}}{D_{r,x'x'} + D_{r,y'y'}} = \frac{2}{K_{r,min}} \left(\frac{K_{r,x'x'}K_{r,y'y'}}{K_{r,x'x'} + K_{r,y'y'}} \right). \quad (2.2)$$

As has been mentioned before, Perrin's analysis is limited to relaxation from a small applied field or response to a small oscillating probe field.

2.2.1 Simulation parameters

The particles are considered permanently magnetized along the z' -axis, and different particle aspect ratios were used in the simulations, as illustrated in Figure 2-1 and summarized in Table 2.1. Three types of simulation runs were performed: (i) equilibrium in a constant magnetic field, (ii) relaxation after switching off an equilibrium field, and

(iii) response to an oscillating magnetic field. All runs were performed using 10^5 non-interacting particles, a time step $\Delta\tilde{t} = 0.01$, and different values of the Langevin parameter ($0.1 \leq \alpha \leq 30$). For the relaxation runs the system was allowed to achieve equilibrium and then the magnetic field was suppressed.

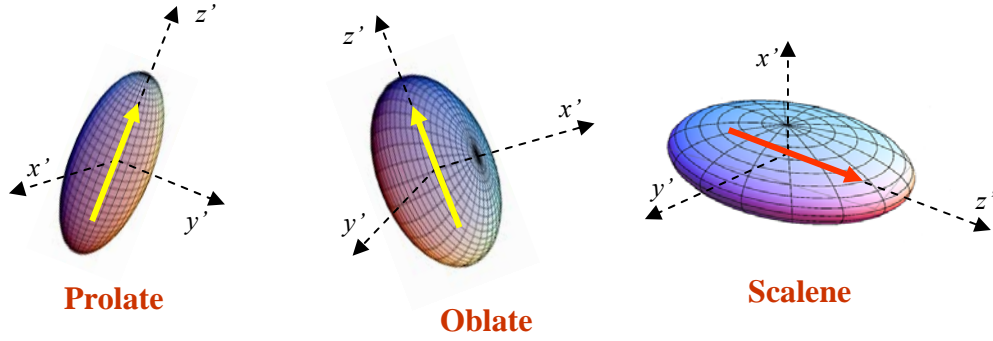


Figure 2-1: Type of ellipsoidal particles used in the simulations.

For the oscillating magnetic field runs the suspension was subjected to an a.c. magnetic field $\mathbf{H} = H_0 \cos(\Omega t) \mathbf{i}_z$ and runs were conducted at dimensionless frequencies, $\tilde{\Omega} = \Omega / D_{r,\max}$, in the range of $10^{-2} - 10^2$. Values for hydrodynamic resistance coefficients were calculated from (1.31) and summarized in Table 2.1.

2.2.2 Simulation results and discussion

Equilibrium simulations were carried out first in order to validate the algorithm. Figure 2-2 shows the dimensionless equilibrium magnetization as a function of the Langevin parameter for the different types of particles. Clearly, the equilibrium magnetization is well described by the Langevin function, Eq. (1.8), independent of the

aspect ratio of the particles. This is to be expected because the energy necessary to rotate the particle into the field direction, which enters into the equilibrium Boltzmann distribution, is a function only of the zenithal angle θ (see Eq. (1.5) and Figure 1-5).

Table 2.1: Aspect ratios and rotational hydrodynamic resistance coefficients of the different types of particles used in the simulations. Here $\tilde{a}_1 = a_1/a_3$, $\tilde{a}_2 = a_2/a_3$, and $\hat{K}_r = K_r/a_3^3$

Type of particle	\tilde{a}_1	\tilde{a}_2	$\hat{K}_{r,x'x'}$	$\hat{K}_{r,y'y'}$	$\hat{K}_{r,z'z'}$
Sphere	1.0	1.0	25.13	25.13	25.13
Prolate	0.1	0.1	3.33	3.33	0.17
Oblate	0.1	1.0	12.04	10.80	10.80
Scalene-1	0.1	0.25	4.06	4.69	0.64
Scalene-2	0.1	0.5	5.76	6.77	2.44
Scalene-3	1.0	0.5	2.44	6.77	5.76

Figure 2-3 shows relaxation of the magnetization after the external field is suppressed. The system is allowed to achieve equilibrium in 10^4 time steps, then the external field is set to zero. The relaxation curves are shifted to higher values of dimensionless time when the aspect ratio of the particle is lower. Hence, prolate shaped particles take longer times relative to the minimum characteristic relaxation time to relax to a new equilibrium state, compared to spherical and oblate particles.

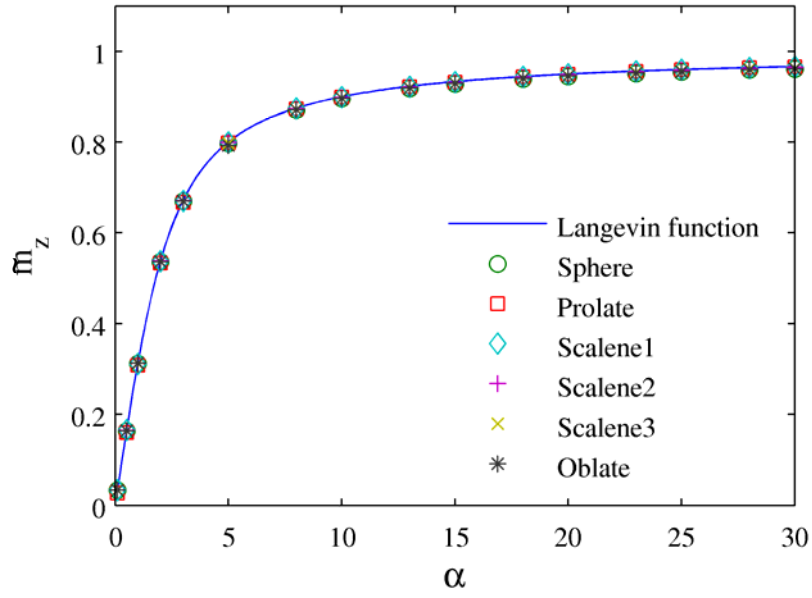


Figure 2-2: Dimensionless equilibrium magnetization as a function of Langevin parameter.

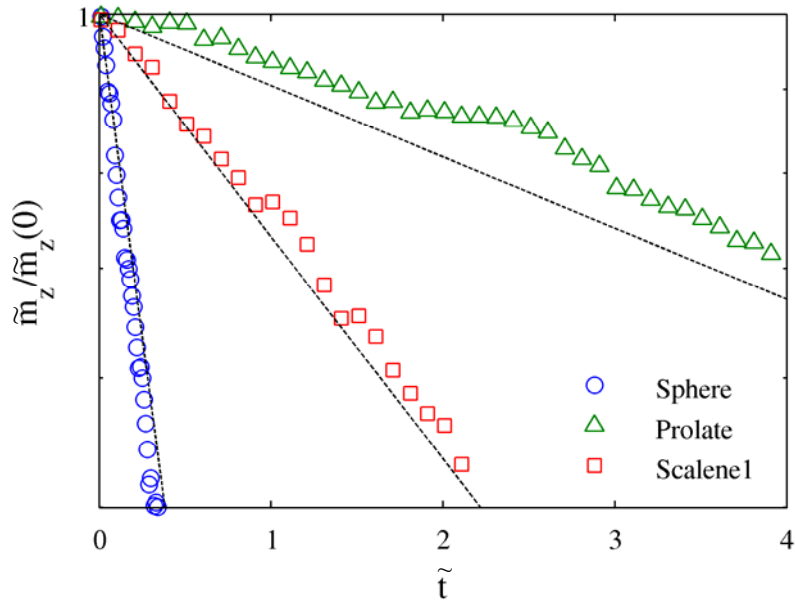


Figure 2-3: Relaxation of dimensionless normalized magnetization for $\alpha = 0.1$. Dashed line represents the Eq. (2.3) with $\tilde{\tau}_{eff}$ from (2.2).

For $\alpha = 0.1$ the magnetization curves show good agreement with Debye's theory, Eq. (1.14), with the particles having an effective relaxation time given by τ_{eff} ; thus, the relaxation of the magnetization in dimensionless form can be written as

$$\tilde{m}_z(t) = \tilde{m}_z(0) \exp\left(-2 \frac{\tilde{t}}{\tilde{\tau}_{eff}}\right). \quad (2.3)$$

Eq. (2.3) can be used to obtain $\tilde{\tau}_{eff}$ from the slopes of the curves in Figure 2-3. Values for $\tilde{\tau}_{eff}$ shown in Table 2.2, agree with Perin's effective relaxation time.

Table 2.2: Dimensionless effective relaxation time from simulations and theory for each type of particle

Type of particle	$\tilde{\tau}_{eff, \alpha=0.1}$	$\tilde{\tau}_{eff, Eq. (2.2)}$
Sphere	1.1 ± 0.03	1.0
Prolate	20.0 ± 2.0	20.2
Oblate	1.0 ± 0.06	1.06
Scalene-1	6.4 ± 0.6	6.89
Scalene-2	2.9 ± 0.6	2.57
Scalene-3	1.4 ± 0.02	1.47

In the case of an external oscillating magnetic field, the dimensionless magnetization for a suspension composed of tri-axial particles has periodic behavior and therefore it can be represented by a Fourier series as

$$\tilde{m}_z = \frac{1}{3} \alpha \sum_{n=1}^{\infty} [\tilde{\chi}'_n \cos(n\tilde{\Omega}\tilde{t}) + \tilde{\chi}''_n \sin(n\tilde{\Omega}\tilde{t})], \quad (2.4)$$

here $n = 1$ denotes the fundamental susceptibility, while $n = 2, 3, 4, \dots$ are the higher order harmonics in $\hat{\chi}$.

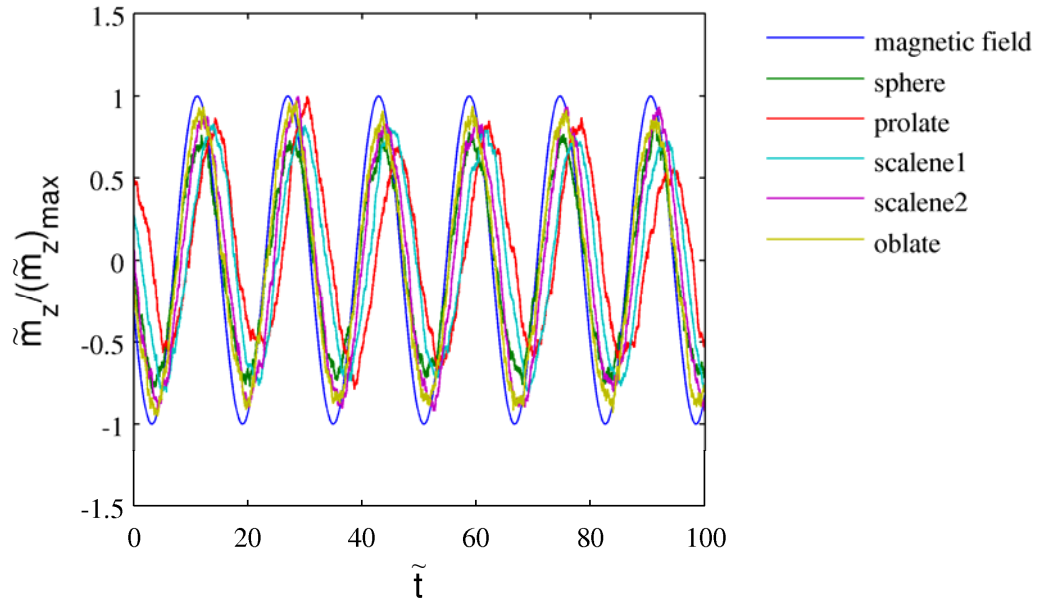


Figure 2-4: Variation of the magnetization with time when an external oscillating magnetic field is applied, for $\alpha = 0.1$ and $\tilde{\Omega} = 0.4$.

For $\alpha = 0.1$ it is possible to obtain the fundamental in-phase and out-of-phase dimensionless dynamic susceptibilities, $\tilde{\chi}'$ and $\tilde{\chi}''$, respectively, by simple integration as Fourier coefficients. Thus,

$$\begin{aligned}\tilde{\chi}' &= \frac{3}{\pi\alpha} \int_0^{2\pi} \tilde{m}_z \cos(\tilde{\Omega}\tilde{t}) d(\tilde{\Omega}\tilde{t}), \\ \tilde{\chi}'' &= \frac{3}{\pi\alpha} \int_0^{2\pi} \tilde{m}_z \sin(\tilde{\Omega}\tilde{t}) d(\tilde{\Omega}\tilde{t}).\end{aligned}\tag{2.5}$$

Eq. (2.5) can be evaluated numerically using simulation results for \tilde{m}_z .

Note that when an oscillating magnetic field is applied, the magnetization of the suspension changes with time following the field oscillations. There exists a phase-lag between the magnetization and the magnetic field, which is dependent on the aspect ratio of the particles and the frequency of the magnetic field, as shown in Figure 2-4.

Figure 2-5 shows dimensionless susceptibilities as a function of dimensionless frequency. All curves have the same shape as Debye's model for particles with only one relaxation time, but particles with aspect ratios less than one shift to the left indicating a slower relaxation process characterized by a higher effective relaxation time, $\tilde{\tau}_{eff}$.

At low frequencies the magnetic field has a characteristic time that is longer than the $\tilde{\tau}_{eff}$ of the particles, then the magnetization is in-phase with the magnetic field and it is independent of the aspect ratio as is observed from $\tilde{\chi}'$ and $\tilde{\chi}''$ values close to one and zero, respectively. As the frequency increases, the characteristic time of the magnetic field is lower than $\tilde{\tau}_{eff}$ and thus those particles with higher $\tilde{\tau}_{eff}$ show out-of-phase and lower values of the dimensionless magnetization.

As expected for particles suspended in a Newtonian fluid, in-phase and out-of-phase susceptibilities vanish at high frequencies, where the particles are unable to follow the

magnetic field fluctuations. It can be seen from the particular case of isotropic particles, Eq. (1.16), where $\lim_{\Omega \rightarrow 0} \chi', \chi'' = 0$.

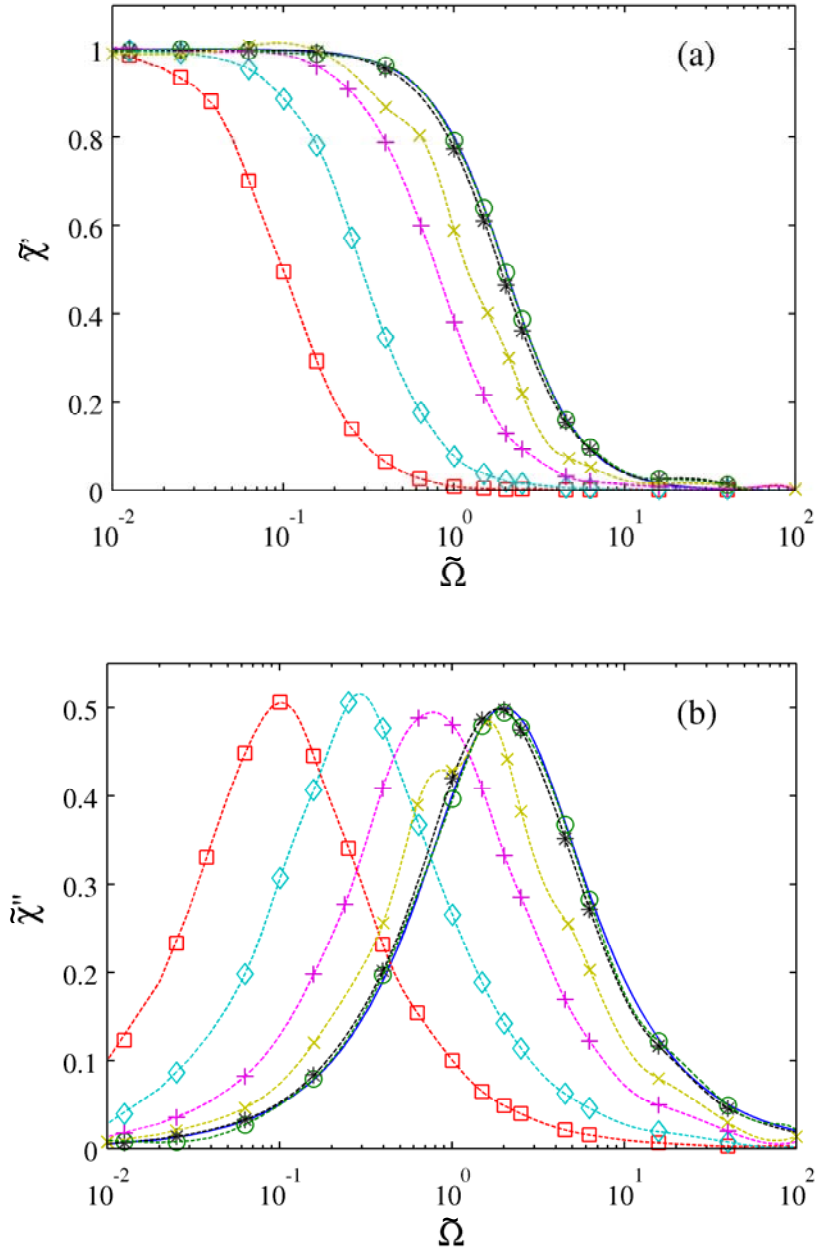


Figure 2-5: Real (a) and imaginary (b) components of the dimensionless complex susceptibility as a function of dimensionless frequency. Solid line represents the Debye's model, Eq. (1.16), and markers from Figure 2-2.

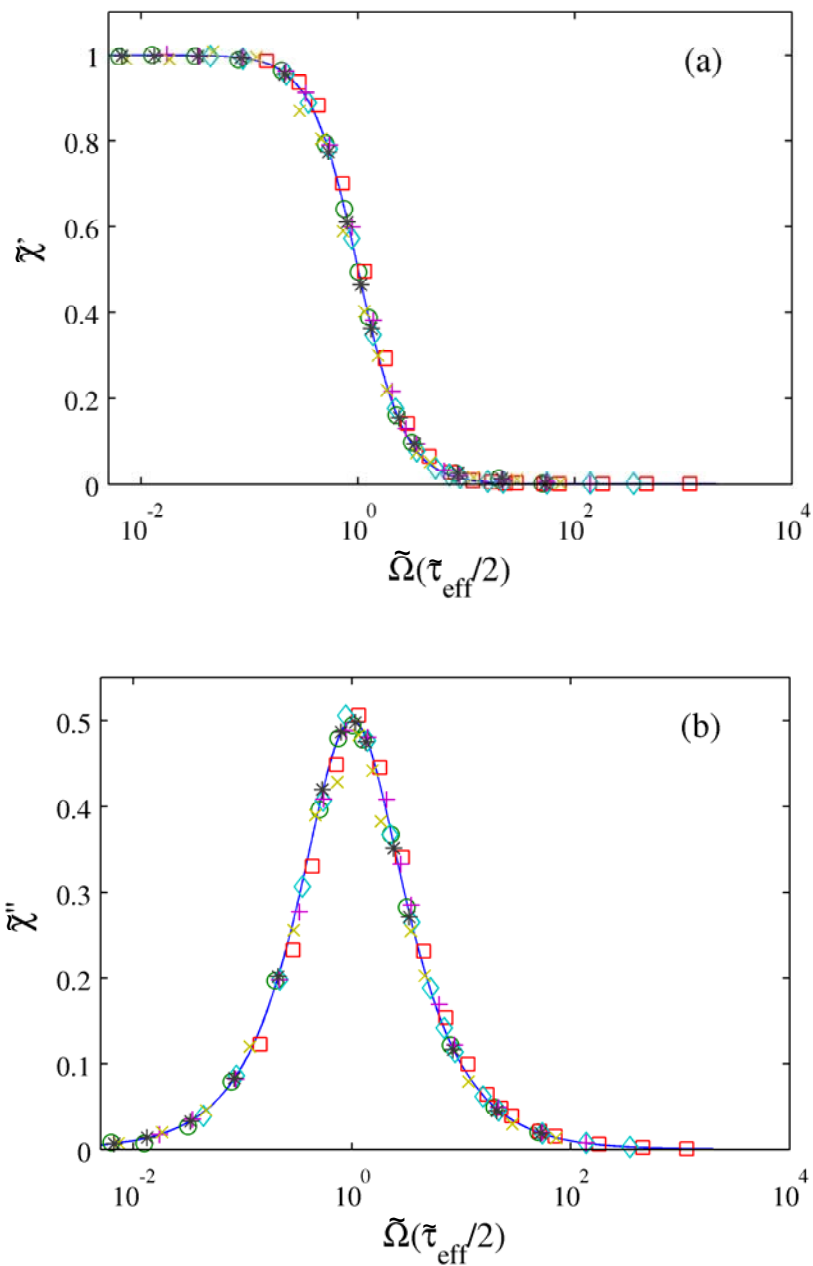


Figure 2-6: Real (a) and imaginary (b) components of the dimensionless complex susceptibility as a function of $\tilde{\Omega}\tau_{\text{eff}}/2$. Symbols from Figure 2-2.

Now, according to these observations and Perrin's analysis the in-phase and out-of-phase susceptibilities may be expressed as

$$\tilde{\chi}' = \frac{1}{1 + (\tilde{\Omega}\tilde{\tau}_{eff}/2)^2}, \quad \tilde{\chi}'' = \frac{(\tilde{\Omega}\tilde{\tau}_{eff}/2)}{1 + (\tilde{\Omega}\tilde{\tau}_{eff}/2)^2}. \quad (2.6)$$

This implies that the dynamic susceptibilities, $\tilde{\chi}'$ and $\tilde{\chi}''$, can be represented by a unique curve when plotted against $\tilde{\Omega}\tilde{\tau}_{eff}/2$. Indeed, as shown in Figure 2-6 the complex susceptibility fits this model independent of the aspect ratio of the particles.

2.3 Magnetization response to strong magnetic fields

For asymmetric top particles in equilibrium with a strong external constant field $\mathbf{H} = H_0 \mathbf{i}_z$, if the field is suppressed the magnetization will relax to a new equilibrium state following exponential decay, which according to Kalmykov and Titov's analysis [44] is given by (in our notation)

$$\tilde{m}_z = L(\alpha_0) \left(\tilde{\mu}_x^2 e^{-2\tilde{t}/\tilde{\tau}_1} + \tilde{\mu}_y^2 e^{-2\tilde{t}/\tilde{\tau}_2} + \tilde{\mu}_z^2 e^{-2\tilde{t}/\tilde{\tau}_3} \right). \quad (2.7)$$

Here $L(\alpha_0)$ is the Langevin function, Eq. (1.8), α_0 is the Langevin parameter for H_0 , and the relaxation times $\tilde{\tau}_1$, $\tilde{\tau}_2$, and $\tilde{\tau}_3$ depend on the diagonal components of the rotational diffusion tensor as follows

$$\tilde{\tau}_1 = \frac{2D_{r,\max}}{D_{r,y'y'} + D_{r,z'z'}}, \quad \tilde{\tau}_2 = \frac{2D_{r,\max}}{D_{r,x'x'} + D_{r,z'z'}}, \quad \tilde{\tau}_3 = \frac{2D_{r,\max}}{D_{r,x'x'} + D_{r,y'y'}}. \quad (2.8)$$

On the other hand, if the suspension is subjected to a magnetic field given by $\mathbf{H} = \mathbf{H}_0 + \mathbf{H}_1$ where $\mathbf{H}_0 = H_0 \mathbf{i}_z$ is a strong d.c. field (bias field) and $\mathbf{H}_1 = \text{Re}\{H_1 e^{j\tilde{\Omega}t}\} \mathbf{i}_z$ is a small a.c. perturbing field (probe field), the magnetization may be approximated by [45].

$$\tilde{m}_z = L(\alpha_0) + \alpha_1 \left[1 - 2 \frac{L(\alpha_0)}{\alpha_0} - L^2(\alpha_0) \right] \text{Re}\{\hat{\chi} e^{j\tilde{\Omega}t}\}, \quad (2.9)$$

where α_1 is the Langevin parameter for H_1 (i.e., $\alpha_1 \ll 1$, which is the linear response condition), and $\hat{\chi}$ is given by three Lorentzians as

$$\hat{\chi} = \frac{\tilde{\mu}_x^2}{1 + j \left[\frac{1}{2} \tilde{\Omega} \tilde{\tau}_1 F(\alpha_0) \right]} + \frac{\tilde{\mu}_y^2}{1 + j \left[\frac{1}{2} \tilde{\Omega} \tilde{\tau}_2 F(\alpha_0) \right]} + \frac{\tilde{\mu}_z^2}{1 + j \left[\frac{1}{2} \tilde{\Omega} \tilde{\tau}_3 F(\alpha_0) \right]}, \quad (2.10)$$

with $F(\alpha_0)$ being a function that relates all $\tilde{\tau}_i$ with the constant bias field

$$F(\alpha_0) = \frac{1 + \alpha_0^2 - \alpha_0^2 \coth \alpha_0}{\alpha_0 \coth \alpha_0 - 1}. \quad (2.11)$$

For large equilibrium and small probe fields, this theory was compared with results from Brownian dynamics simulations, showing that Eqs. (2.7) and (2.9) are correct for the conditions proposed.

2.3.1 Simulation parameters

To verify the models proposed, the particles were considered permanently magnetized along an arbitrary direction such as $\tilde{\mu}_{x'} = \tilde{\mu}_{y'} = \tilde{\mu}_{z'}$, and a “toy” scalene particle, characterized by three different hydrodynamic resistance coefficients, i.e. $\hat{K}_{x',x'} = 10$, $\hat{K}_{y',y'} = 1.0$, and $\hat{K}_{z',z'} = 0.1$, was used in order to separate the contribution of the corresponding relaxation modes to the transient $\tilde{m}_z(t)$. All runs were performed using 10^5 non-interacting particles, a time step $\Delta\tilde{t} = 0.01$, and different values of the Langevin parameter ($\alpha_0 = 1, 10, 100$ and $\alpha_1 = 0.1$). For relaxation runs the system was allowed to achieve equilibrium and then the magnetic field was suppressed. For oscillating magnetic field runs the suspension was subjected to a strong bias field \mathbf{H}_0 until achieving equilibrium, then a small oscillating field \mathbf{H}_1 was imposed and runs were conducted at dimensionless frequencies in the range of 10^{-2} to 10^2 .

2.3.2 Simulation results and discussion

Figure 2-7 shows the normalized dimensionless magnetization as a function of dimensionless time for different values of the Langevin parameter. Clearly, the anisotropic magnetization relaxation is well described by (2.7) for large α_0 parameters. Furthermore, the expressions for the relaxation times in (2.8) are the same of those given by Perrin [36], thus indicating that (2.7) can predicts results for magnetization relaxation even at small values of the Langevin parameter, which agrees with Weber’s model [41] and Small and Isenberg [40] for fluorescence depolarization. Thus, despite the strength of the magnetic field at the initial equilibrium state, the magnetization decay is well

represented by three exponentials, contrary to the five exponentials obtained analytically by Chuang and Eisenthal [42], and Erhenberg and Rigler [43] in the case of anisotropic fluorescence depolarization after an instantaneous exciting light pulse.

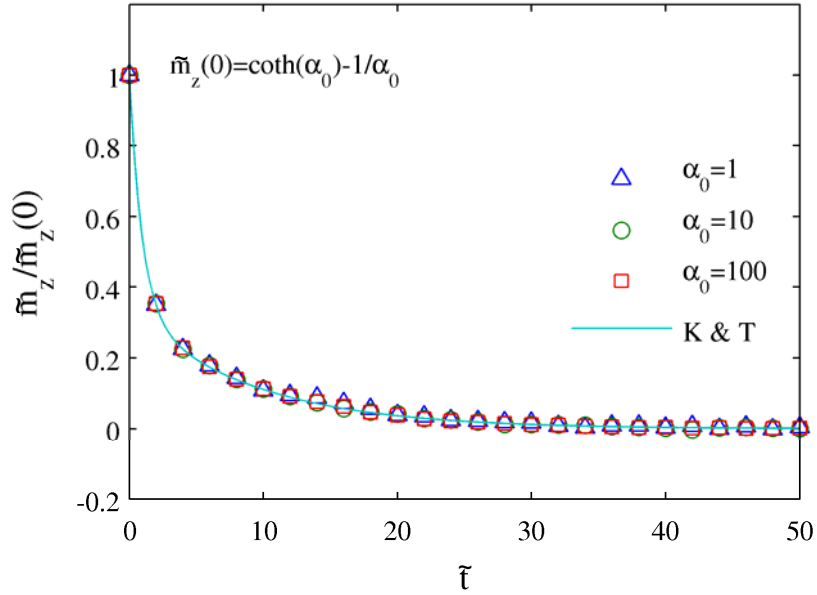


Figure 2-7: Relaxation of dimensionless normalized magnetization for different values of Langevin parameter and comparison with Kalmykov and Titov’s model (K & T).

On the other hand, a comparison of the real and imaginary parts of the dimensionless complex susceptibility $\hat{\chi}(\tilde{\Omega})$ using the equation (2.10) and results from simulations are given in Figure 2-8. The numerical results for $\alpha = 0.1$ are in agreement with those from the effective relaxation time solution for a high bias field strength parameter α_0 at low and high frequencies. At intermediate frequencies the results for the in-phase and out-of-phase susceptibilities obtained from (2.10) are slightly higher than those from simulations, thus (2.9) will predict higher values of the magnetization of the suspension.

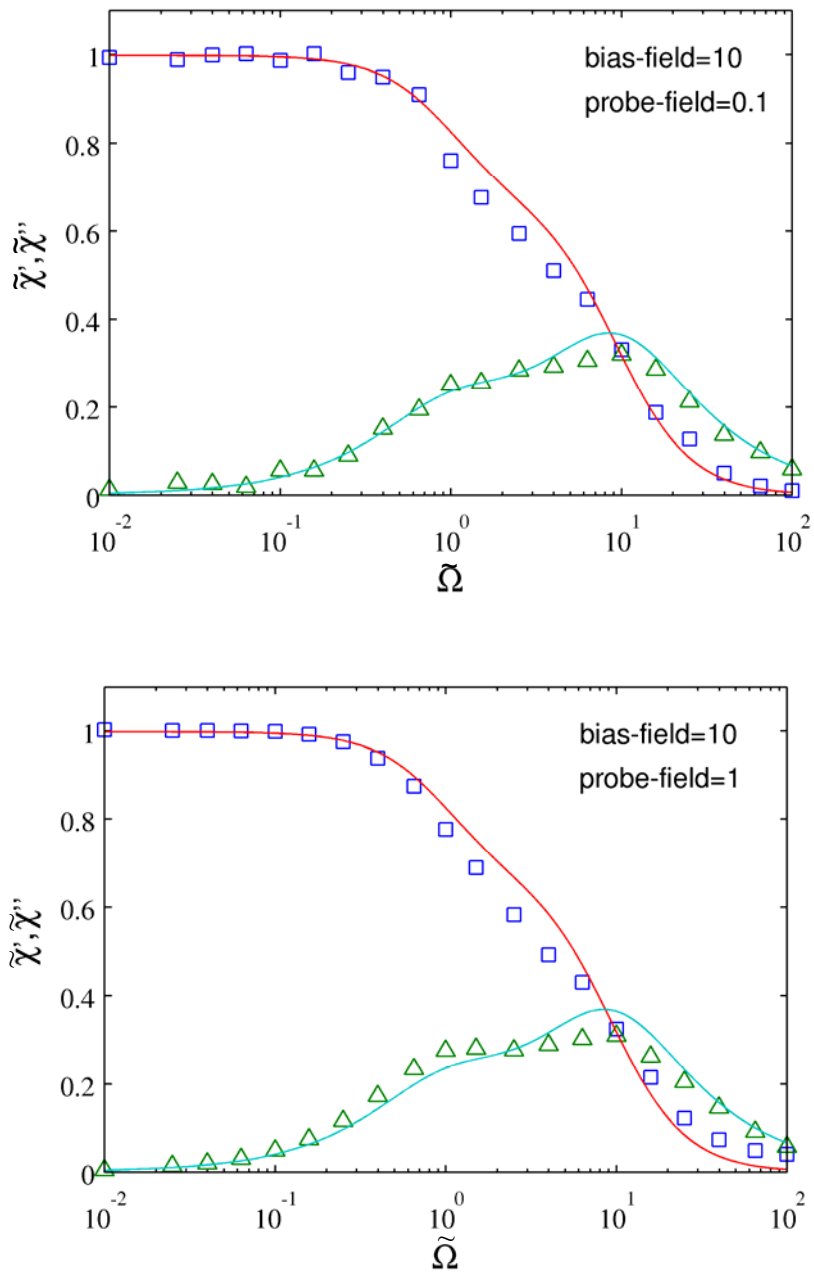


Figure 2-8: Real and imaginary components of the dimensionless complex susceptibility as a function of the dimensionless frequency for different probe field strengths. Markers for simulation results and solid lines for Kalmykov and Titov's model.

Similar behavior is achieved with $\alpha_1 = 1$, showing that (2.10) is capable to predicts the complex susceptibility of suspensions of asymmetric top particles for slightly higher probe fields.

2.4 Conclusions

The magnetization of suspensions of non-interacting tri-axial permanently magnetized particles under d.c. and a.c. external magnetic fields was studied. The inertialess approximation of the Langevin equation was solved numerically and simulated in order to obtain the dynamic magnetic behavior of the suspension when it is subjected to an external magnetic field and the carrier fluid is a Newtonian liquid.

The results show that the equilibrium magnetization of the suspension is independent of the aspect ratio of the particles and is described by the Langevin function. Furthermore, relaxation from small and high fields shows the magnetization being characterized by effective relaxation times as shown by Perrin [36], Coffey *et al.* [37], and Kalmykov and Titov [44], respectively. Also, simulations demonstrate that in-phase and out-of-phase susceptibilities can be represented by a unique function using the effective relaxation time, $\tilde{\tau}_{eff}$, independent of the aspect ratio of the particle for small external magnetic fields, and that is well described by three Lorentzians for small probe fields superimposed over a strong bias field.

These results are of great interest because recent studies from atmospheric science, toxicology, and epidemiology have shown the need to better characterize and understand the formation process of the nanometric fraction of particulate matter, due to its possible effects on the environment and on human health [46]. Consequently, there is an

increasing demand for diagnostics able to determine physical and chemical properties of particles in the nanosize range. Thus, by measuring the characteristic time of depolarization processes, as for example by optical methods based on time-dependent fluorescence polarization, it is possible to determine the particle's size.

3 MAGNETOVISCOSITY OF DILUTE SUSPENSIONS OF MAGNETIC ELLIPSOIDS IN CONSTANT MAGNETIC FIELDS

For a collection of particles with embedded magnetic dipoles suspended in a Newtonian fluid in simple shear flow it is known that if an external magnetic field is applied the particles will rotate relative to the fluid resulting in a change in the viscosity of the suspension. This phenomenon is known as the magnetoviscous effect and the part of the viscosity resulting from the action of the field as the magnetoviscosity [47] or rotational viscosity [2, 48]. This effect is in addition to the increase in viscosity for force- and torque-free suspended particles, first estimated by Einstein [14, 49] for a suspension of rigid spherical particles.

The influence of an external magnetic field on the viscosity of a magnetic fluid was first observed experimentally by McTague [5] and Rosensweig *et al.* [6]. While McTague focused only on the magnetic effect on the capillary viscosity of highly diluted ferrofluids, Rosensweig considered the effect of shear rate, showing that the suspension has shear thinning behavior. Later, a theoretical description was developed by Hall and Busenberg [50], who considered a suspension of ferromagnetic spherical particles but neglected Brownian motion. Based on an energy balance, their results predict that the effective viscosity of the suspension in shear flow depends on both the direction and magnitude of the external magnetic field through

$$\eta_{eff} = \eta_0 \left(1 + \frac{5}{2} \phi + \frac{3}{2} \phi \sin^2 \phi_s \right),$$

$$\sin^2 \phi_s = \frac{1}{2} \left(1 + \xi^2 \right) - \left[\frac{1}{4} \left(1 + \xi^2 \right)^2 - \xi^2 \sin^2 \beta \right]^{1/2},$$
(3.1)

where ϕ is the volume fraction of particles in solution, η_0 is the viscosity of the carrier liquid, $\xi = (\mu_0 \mu H) / (4\pi \eta_0 a^3 \dot{\gamma})$ represents the ratio between the magnetic torque and the hydrodynamic torque acting on a particle, and β is the angle between the magnetic field and vorticity.

Later, Shliomis [48] argued that viscosity values obtained from (3.1) were not in agreement with the experimental results of McTague due to the fact that Brownian rotation was neglected. Shliomis [48] derived an expression for a suspension of magnetized Brownian spherical particles for the case of low shear rate and short magnetization relaxation time, $\omega_f \tau_B \ll 1$, which is given by

$$\eta^m = \frac{3}{2} \phi \eta_0 \left(1 + \frac{5}{2} \phi \right) \frac{\alpha - \tanh \alpha}{\alpha + \tanh \alpha} \sin^2 \beta,$$
(3.2)

where η^m is the magnetic part of the viscosity (which we shall refer to as the magnetoviscosity), α is the Langevin parameter, and β is the angle between the magnetic field and vorticity. Although (3.2) includes the effect of rotational Brownian motion it neglects the effect of shear rate, hence it cannot fully describe the results of Rosensweig *et al.* [6]. However, more recently Shliomis [51] obtained an expression for the magnetoviscosity of dilute ferrofluids for finite shear rates, $\omega_f \tau_B \geq 1$. The viscosity

equation was derived from a phenomenological magnetization equation, which in turn was derived from irreversible thermodynamics, employing the effective-field method, resulting in the following

$$\begin{aligned}\eta^m &= \frac{3}{2}\eta_0\phi\frac{\xi L(\xi)}{2+\xi L(\xi)}, \\ \sqrt{\alpha^2-\xi^2} &= \frac{2\omega_f\tau_B\xi}{2+\xi L(\xi)},\end{aligned}\tag{3.3}$$

where ξ is analogous to the Langevin parameter for an effective magnetic field, and $L(\xi)$ is the Langevin function as given by (1.8). According to Shliomis, this equation yields a quite satisfactory description of magnetoviscosity in the whole region of magnetic field strength and shear rate.

Working independently, Brenner and Weissman [52] numerically solved the Smoluchowski equation for the orientational distribution function and developed a dynamical theory of the rheology of suspensions of non-interacting dipolar Brownian spherical particles. They derived expressions for the stress tensor and showed the effect on the intrinsic viscosity of both the external field strength and shear rate, parameterized through the rotational Péclet number $Pe_r = \dot{\gamma}/D_r$, where $\dot{\gamma}$ is the shear-rate of the fluid and D_r is the rotational diffusion coefficient of the particle. Note that in Brenner and Weissman's work a factor of 1/2 is included in their rotational Péclet number. In addition to numerical solutions, they provide several analytic solutions using a perturbation method for some limited ranges of the parameters studied, such as weak external field

and dominant shear rate. Their results show a discrepancy with experimental data which is attributed to the fact that the suspension was assumed sufficiently dilute to preclude hydrodynamic and magnetic interactions between the particles.

As mentioned in Chapter 1, nonspherical particles have received recent attention due to their applicability in many different fields of modern technology [24, 28, 53-57]. For example, Satoh [27] studied the effect of magnetic and shear flow fields on the orientation distribution and viscosity of dilute spherocylinder dispersions when the magnetic moment is parallel to the particle symmetry axis for $Pe_r \geq 1$ and $\alpha \geq 1$. The governing equation was solved by means of Galerkin's method and his results show that for a magnetic field perpendicular to the local vorticity of the fluid, the orientation distribution is dependent on the relative ratio between magnetic field and shear rate, and that particles with extreme aspect ratio lead to a larger increase in viscosity. On the other hand, Strand and Kim [58] presented a numerical method, employing the Galerkin method, for calculating the orientation distribution function and thus rheological properties of dilute suspensions of dipolar Brownian axisymmetric particles subjected to shear and external magnetic fields. They studied the effect of the orientation of the magnetic field respect to the local vorticity on the intrinsic effective viscosity, founding that particles with extreme aspect ratio exhibit a maximum value of effective viscosity for intermediate shear rates at selected field orientations. Recently, Satoh *et al.* [59, 60] analyzed the case with the magnetic moment normal to the particle symmetry axis. Furthermore, Asokan and Ramamohan [54] computed rheological parameters of suspensions of noninteracting spheroids in a simple shear flow under an external force

field. They found chaotic fluctuations in the apparent viscosity when the external field is periodic in time.

The purpose of this chapter is to present rotational Brownian dynamics simulations for the intrinsic magnetoviscosity $[\eta^m]$ of a magnetic fluid composed of non-interacting tri-axial ellipsoidal permanently magnetized particles suspended in a Newtonian fluid and subjected to both magnetic fields and simple shear flow in order to study the effect of the aspect ratio of the particles on the intrinsic magnetoviscosity of the suspension.

3.1 Calculation of the magnetoviscosity of the suspension

The viscous (or deviatoric) stress tensor $\boldsymbol{\tau}$ for a suspension of dipolar particles subjected to an external field is characterized by both a symmetric and an antisymmetric part [61, 62]

$$\boldsymbol{\tau} = \boldsymbol{\tau}^s + \boldsymbol{\tau}^a. \quad (3.4)$$

The antisymmetric component $\boldsymbol{\tau}^a$ arises from the angular slip velocity between the local angular velocity of the suspension and the average angular velocity of the particles [61]. This slip velocity appears as a result of hindered rotation of the particles due to external couples, resulting in a greater rate of mechanical energy dissipation, and hence, a larger apparent viscosity [50, 63].

The antisymmetric component of the viscous stress tensor due to the action of magnetic couples in a dilute suspension can be obtained as follows: The spin velocity $\boldsymbol{\Omega}$ in the ferrofluid is governed by the internal angular momentum equation

$$\rho I \frac{D\boldsymbol{\Omega}}{Dt} = \nabla \cdot \mathbf{C} + \mathbf{T}_x + \mathbf{T}_{ext} \quad (3.5)$$

where I is the moment of inertia density of the suspension, \mathbf{C} is the couple stress tensor density that represents the diffusion of internal angular momentum between contiguous material elements, \mathbf{T}_x denotes the pseudovector associated to the antisymmetric stress tensor, and \mathbf{T}_{ext} is the external couple density acting on the structured continuum.

In order that the suspension be considered as a continuum, it must satisfy the inequality $(a/L) \ll 1$, where L is the length scale on which the velocity field varies, and a is the characteristic length of the particles. Whence, in the continuum limit, namely where $(a/L) \rightarrow 0$ (since the size of the particles in a magnetic fluid), and the assumption of a dilute suspension, the internal angular momentum equation becomes couple-stress-free and inertia-free; thus, from (3.5) $\mathbf{T}_x + \mathbf{T}_{ext} = \mathbf{0}$ [62].

According to Brenner [64], for a two-phase system, neglecting rotary inertial effects on the particles, the external couple density exerted on the macrocontinuum would be given as $\mathbf{T}_{ext} = (\sum_i \mathbf{T}_{m,i})/V$, where \mathbf{T}_m is the magnetic torque acting on each particle. Since the antisymmetric part of the stress tensor $\boldsymbol{\tau}^a$ can be found from \mathbf{T}_x , using the following relationship employing the alternating tensor $\boldsymbol{\varepsilon}$: $\boldsymbol{\tau}^a = \frac{1}{2} \boldsymbol{\varepsilon} \cdot \mathbf{T}_x$, then

$$\boldsymbol{\tau}^a = -\frac{n}{2} \langle \boldsymbol{\varepsilon} \cdot \mathbf{T}_m \rangle, \quad (3.6)$$

in which n is the number density of particles, and the angular brackets denote an average over the ensemble of particles in the suspension.

For the simple shear flow given in (1.21), the apparent viscosity of the suspension due to the antisymmetric part of the viscous stress tensor is given by $\eta_{zy}^m = \tau_{zy}^a / \dot{\gamma}$, which is referred to as the magnetoviscosity of the suspension. Therefore, from the Péclet number definition

$$\eta_{zy}^m = \frac{\tau_{zy}^a}{\text{Pe}_r D_{r,\max}}. \quad (3.7)$$

Using the Stokes-Einstein equation for $D_{r,\max}$, and Eq. (3.6), we obtain that

$$\eta_{zy}^m = -\frac{n}{2} \eta_0 \frac{\alpha}{\text{Pe}_r} K_{r,\min} \left\langle \boldsymbol{\varepsilon} \cdot (\tilde{\boldsymbol{\mu}} \times \tilde{\mathbf{H}}) \right\rangle_{zy}, \quad (3.8)$$

where the volume fraction of particles ϕ can be expressed as $\phi = nV_p$, with

$V_p = \frac{4}{3} \pi a_1 a_2 a_3$ being the volume of a tri-axial particle. Thus, (3.8) becomes

$$\eta_{zy}^m = -\phi \eta_0 \frac{3}{8\pi \tilde{a}_1 \tilde{a}_2} \frac{\alpha}{\text{Pe}_r} \hat{K}_{r,\min} \left\langle \boldsymbol{\varepsilon} \cdot (\tilde{\boldsymbol{\mu}} \times \tilde{\mathbf{H}}) \right\rangle_{zy}, \quad (3.9)$$

where $\tilde{a}_1 = a_1/a_3$, $\tilde{a}_2 = a_2/a_3$, and $\hat{K}_{r,\min} = K_{r,\min}/a_3^3$. For a dilute suspension, the

intrinsic magnetoviscosity $[\eta_{zy}^m]$ is defined as

$$[\eta_{zy}^m] = \lim_{\phi \rightarrow 0} \frac{\eta_{zy}^m}{\phi \eta_0}. \quad (3.10)$$

Thus, from (3.9)

$$[\eta_{zy}^m] = -\frac{3}{8\pi \tilde{a}_1 \tilde{a}_2} \frac{\alpha}{\text{Pe}_r} \hat{K}_{r,\min} \left\langle \boldsymbol{\varepsilon} \cdot (\tilde{\boldsymbol{\mu}} \times \tilde{\mathbf{H}}) \right\rangle_{zy}. \quad (3.11)$$

Equation (3.11) furnishes $[\eta_{zy}^m]$ as a function of the Langevin parameter, the dimensionless shear-rate expressed as a rotational Péclet number, the particle shape, and the average orientation of the particles. It is important to note that the aspect ratio is defined relative to the semiaxis along the magnetic dipole moment of the particle.

To calculate the time evolution of the intrinsic magnetoviscosity by numerical simulation it is necessary to express (3.11) in terms of the Euler parameters of the particles. Using the transformation matrix \mathbf{A} , the intrinsic magnetoviscosity of the suspension, subjected to a magnetic field along the z -direction, can be obtained from

$$[\eta_{zy}^m] = \frac{3}{8\pi \tilde{a}_1 \tilde{a}_2} \frac{\alpha}{\text{Pe}_r} \hat{K}_{r,\min} \left\langle 2(e_2 e_3 - e_0 e_1) \tilde{H}_z \right\rangle. \quad (3.12)$$

Thus, from (3.12) in conjunction with (1.38) and (1.39), the evolution with time of the intrinsic magnetoviscosity is obtained.

For the present, the influence of the aspect ratio of the particles on the magnetoviscosity of the suspension, when it is under an external magnetic field, is studied.

3.2 Simulation parameters

Various particle aspect ratios were used in the simulations, as summarized in Table 2.1 (except Scalene-3). The suspension was subjected to a constant magnetic field $\mathbf{H} = H\mathbf{i}_z$ and to a simple shear flow as given by (1.21). All runs were performed starting from a random configuration, using 10^5 noninteracting particles, a time step of $\Delta\tilde{t} = 0.01$, Langevin parameters of $0.1 \leq \alpha \leq 100$, and shear rates of $0.1 \leq \text{Pe}_r \leq 100$.

3.3 Results and discussion

Figure 3-1 shows the intrinsic magnetoviscosity of a suspension of spherical particles as a function of the Langevin parameter and Péclet number. The figure shows that the intrinsic magnetoviscosity approaches the saturation value of $3/2$ at high field, $\alpha > 20$, where the magnetic field dominates the Brownian and hydrodynamic torques, resulting in particles with their magnetic dipole moments almost aligned in the field direction, and leading to a complete hindrance of the particle's rotation. For $\alpha \gg 1$ the particle achieves a stable, non-rotating state in which $\boldsymbol{\omega} = \mathbf{0}$; thus, for a spherical particle neglecting the Brownian torque, we obtain from (1.38) that

$$\frac{d\tilde{\boldsymbol{\Phi}}}{dt} = \text{Pe}_r \tilde{\boldsymbol{\omega}}_f + \alpha (\tilde{\boldsymbol{\mu}} \times \tilde{\mathbf{H}}). \quad (3.13)$$

Note that in the particular case of an isotropic particle the angular momentum equation can be expressed relative to space-fixed axes. The solution of this differential equation furnishes the particle orientation as a function of time. Therefore, in steady state and taking into account that $|\tilde{\boldsymbol{\mu}}|=1$, this unique terminal condition is characterized by the orientation vector

$$\tilde{\boldsymbol{\mu}} = \frac{\text{Pe}_r}{2\alpha} \mathbf{i}_y + \left[1 - \left(\frac{\text{Pe}_r}{2\alpha} \right)^2 \right]^{1/2} \mathbf{i}_z. \quad (3.14)$$

As $\alpha \rightarrow \infty$ the embedded dipole exhibits a preferred orientation along the magnetic field direction, $\tilde{\boldsymbol{\mu}} = \mathbf{i}_z$, and the orientational distribution function becomes the Dirac delta function [64]. On the other hand, at low fields, the hydrodynamic torque dominates and the particles are able to rotate with the fluid leading to a decrease in the intrinsic viscosity.

For $\text{Pe}_r \ll 4$ (corresponding to $\omega_f \tau_B \ll 1$ in Shliomis' analysis) (3.2) agrees with the results obtained from our simulations in the low- and high- α limits, but deviates from these for intermediate α . This discrepancy is due to an approximate phenomenological equation for the change in the suspension magnetization vector used to derive (3.2) (i.e., the so-called magnetization relaxation equation, which is a generalization of the Debye's relaxation equation), valid for any magnetic field magnitude but only small vorticities, as follow

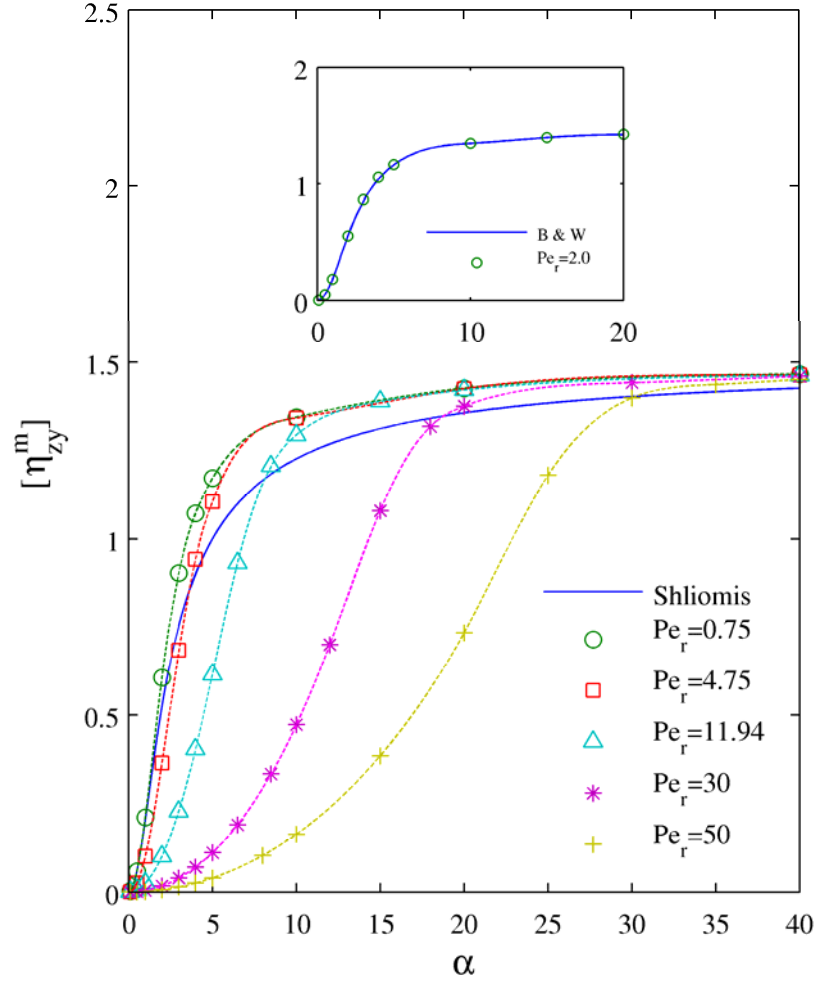


Figure 3-1: Intrinsic magnetoviscosity of a suspension of spherical particles as a function of Langevin parameter for different values of rotational Péclet number, and comparison with results from [48]. Inset, comparison with results from Brenner and Weissman (B & W) [52].

$$\frac{d\mathbf{m}}{dt} = \boldsymbol{\omega}_f \times \mathbf{m} - \frac{1}{\tau_B} (\mathbf{m} - \mathbf{m}_{eq}) - \frac{1}{6\eta_0\phi} \mathbf{m} \times (\mathbf{m} \times \mathbf{H}) \quad (3.15)$$

where \mathbf{m} is the magnetic fluid magnetization and \mathbf{m}_{eq} its equilibrium value as given by the Langevin function.

As shown later by Shliomis [51], other magnetization equations obtained by introducing the concept of an “effective” magnetic field, and applicable for large

deviations from equilibrium, result in different dependence of the magnetic viscosity on the magnetic-field strength. On the other hand, our results are in excellent agreement with those of Brenner and Weissman [52] for $Pe_r = 2.0$.

For higher Pe_r , (3.2) is unable to describe the behavior of the suspension and the results show a decreased effect of α on the viscosity. Moreover, the simulations do not predict a hysteresis of the magnetoviscosity at high shear ($Pe_r > 24$) and high field as was calculated by Shliomis [48] and He *et al.* [47] using the ferrohydrodynamic equations. Again, the use of an approximate magnetization relaxation equation seems to be to blame.

As seen in Figure 3-1, the intrinsic magnetoviscosity increases with the magnetic field strength until it achieves a saturation value, for which the rotational motion of the particles is prevented by the magnetic field. This condition is achieved at lower applied fields (i.e., lower values of α) as the Péclet number decreases, i.e. where Brownian motion dominates the shear forces. As Pe_r increases, the larger shear rate forces the particles to rotate out of alignment with the magnetic field; hence the magnetic field strength for the suppression of the rotational motion of the particles increases.

Figure 3-2 illustrates the effect of shear rate on the intrinsic magnetoviscosity. At low shear rates $[\eta_{zy}^m]$ remains constant up to a critical value of Pe_r , which increases as α increases. At higher shear rates the intrinsic viscosity decreases to zero, indicating shear thinning behavior, as predicted by Brenner and Weissman [52], and observed experimentally by Rosensweig *et al.* [6].

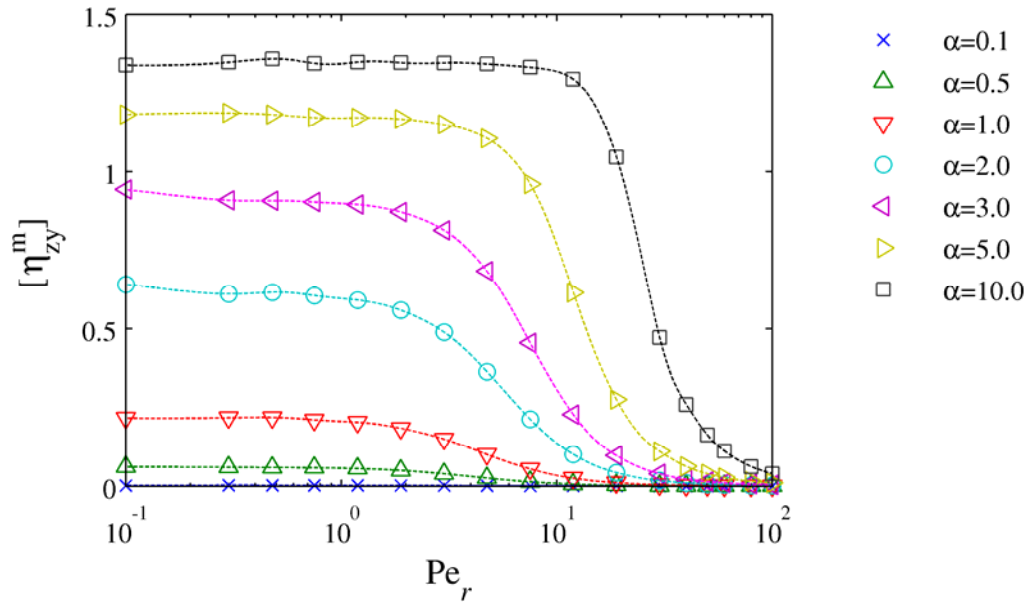


Figure 3-2: Intrinsic magnetoviscosity of a suspension of spherical particles as a function of rotational Péclet number for different values of Langevin parameter.

In the case of ellipsoidal particles the aspect ratio has a significant effect on the viscosity of the suspension. Figure 3-3 shows this as a function of the Langevin parameter for a value of $Pe_r/K_{r,\min} = 5.0$. The parameter $Pe_r/K_{r,\min}$ was used in order to compare results under similar flow conditions. As was the case for spherical particles, the intrinsic magnetoviscosity increases with the strength of the magnetic field, approaching a saturation state. Saturation is achieved faster when the aspect ratio of the particles is lower owing to the decreased rotational hydrodynamic resistance perpendicular to the axis along the magnetic dipole moment, as can be determined from (3.19).

Figure 3-4 shows the intrinsic magnetoviscosity as a function of Péclet number for a Langevin parameter of 3.0. It is seen that at low values of Pe_r , the intrinsic

magnetoviscosity is higher as the aspect ratio decreases and tends to zero at high values of Pe_r , as for spherical particles.

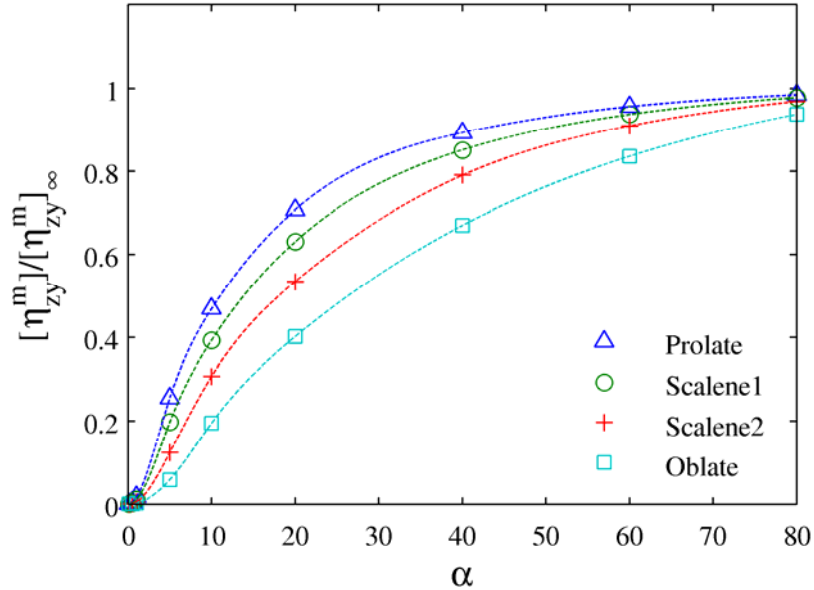


Figure 3-3: Intrinsic magnetoviscosity of suspensions of ellipsoidal particles as a function of Langevin parameter for $Pe_r / K_{r,\min} = 5.0$. Here $[\eta^m_{zy}]_\infty$ is the intrinsic viscosity for $\alpha \rightarrow \infty$.

For suspensions of ellipsoidal particles, the intrinsic magnetoviscosity also exhibits a critical value of Péclet number above which the viscosity decreases, and which shifts towards higher values as the aspect ratio of the particles increases. For example, a suspension of prolate shaped particles achieves this critical value at a lower rate of strain, relative to the maximum rotational diffusion coefficient, than a suspension of oblate particles.

As was mentioned above, if an external magnetic field is applied the particles will rotate relative to the fluid resulting in a change in the viscosity of the suspension.

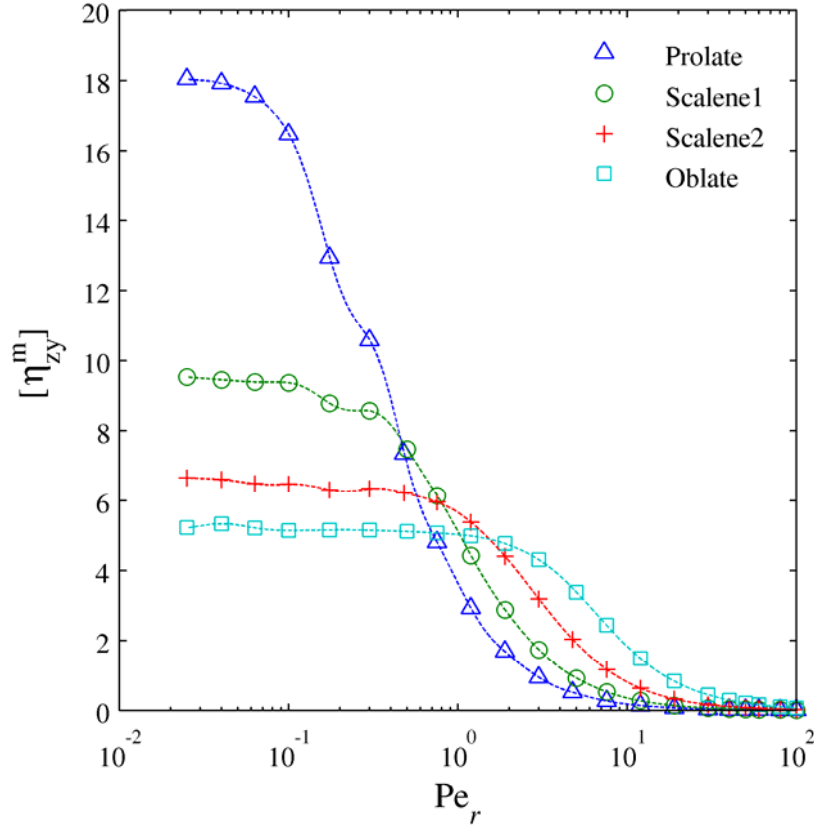


Figure 3-4: Intrinsic magnetoviscosity of suspensions of ellipsoidal particles as a function of rotational Péclet number for $\alpha = 3.0$.

Thus, when a magnetic field is applied, it turns the particle increasing the z -component of the magnetic dipoles, and then the particle rotates tending to align its magnetic dipole moment with the external field. This rotation can be separated into individual rotations about the primed axes. Rotations around the z' -axis do not contribute to any change in the alignment with the magnetic field. Therefore, the alignment process can be represented by a combination of individual rotations about the x' and y' -axis, i.e., the relaxation motion is independent of rotation around the magnetic dipole.

Results from simulations suggest that it is possible to fit the data to a unique curve by using an effective rotational diffusion coefficient $D_{r,\text{eff}}$ instead of $D_{r,\text{max}}$ to define an

effective Péclet number, $Pe_{r,eff} = Pe_r(D_{r,max}/D_{r,eff})$, where $D_{r,eff}$ is obtained from averaging the rotational diffusion tensor, \mathbf{D}'_r , around the z' -axis of the particle. The average rotational diffusion tensor with respect to rotation around the z' -axis, $\langle \mathbf{D}'_r \rangle$, can be obtained from [65]

$$\langle \mathbf{D}'_r \rangle = \int_0^{2\pi} f(\phi) (\mathbf{A}_R \cdot \mathbf{D}'_r \cdot \mathbf{A}_R^T) d\phi, \quad (3.16)$$

where $f(\phi) = 1/(2\pi)$ is the assumed homogeneous orientational distribution function, and \mathbf{A}_R is the rotation matrix.

The corresponding rotation matrix, \mathbf{A}_R , is given by [22]

$$\mathbf{A}_R = \begin{bmatrix} \cos \phi & \sin \phi & 0 \\ \sin \phi & \cos \phi & 0 \\ 0 & 0 & 1 \end{bmatrix}. \quad (3.17)$$

The average rotational diffusion tensor for an orthotropic particle, after averaging, becomes

$$\langle \mathbf{D}'_r \rangle = \mathbf{i}_z \mathbf{i}_z D_{\parallel} + (\mathbf{I} - \mathbf{i}_z \mathbf{i}_z) D_{\perp}, \quad (3.18)$$

where

$$D_{\perp} = \frac{1}{2}(D_{r,x'x'} + D_{r,y'y'}) \quad \text{and} \quad D_{\parallel} = D_{r,z'z'}. \quad (3.19)$$

The coefficients represented by the subscripts \perp and \parallel pertain, respectively, to rotations about axes perpendicular and parallel to the z' -axis of the particle, thus, $D_{r,\text{eff}} = D_{\perp}$.

As shown in Figure 3-5, if the Péclet number is defined with respect to $D_{r,\text{eff}}$, the normalized intrinsic magnetoviscosity, $[\eta_{zy}^m]/[\eta_{zy}^m]_0$, of suspensions of ellipsoidal particles exhibits similar behavior to that of spherical particles for low Langevin parameters. In this case, because the magnetic torque is not strong enough to align the dipole moments with the field, the particles are able to rotate more or less freely with the shear flow exhibiting an almost isotropic orientational distribution, independent of the aspect ratio. On the other hand, for $\alpha = 10$, Figure 3-5 shows that the results for ellipsoidal particles deviate from those for spherical particles for $\text{Pe}_{r,\text{eff}} > 3.0$.

At higher α the particles tend to align with the magnetic field, thus, for low $\text{Pe}_{r,\text{eff}}$, the results show good agreement independent of the aspect ratio. At higher $\text{Pe}_{r,\text{eff}}$, the particles rotate out of alignment with the magnetic field, but owing to the effect of the shear-torque on ellipsoidal particles, they are preferably oriented in the direction of maximum strain, i.e. at an angle of $\pi/4$ with respect to the xz -plane and in the flow direction (the yz -plane).

This behavior was first shown by Jeffery [66] who solved analytically the motion of an ellipsoidal particle (an axisymmetric particle) immersed in a viscous fluid.

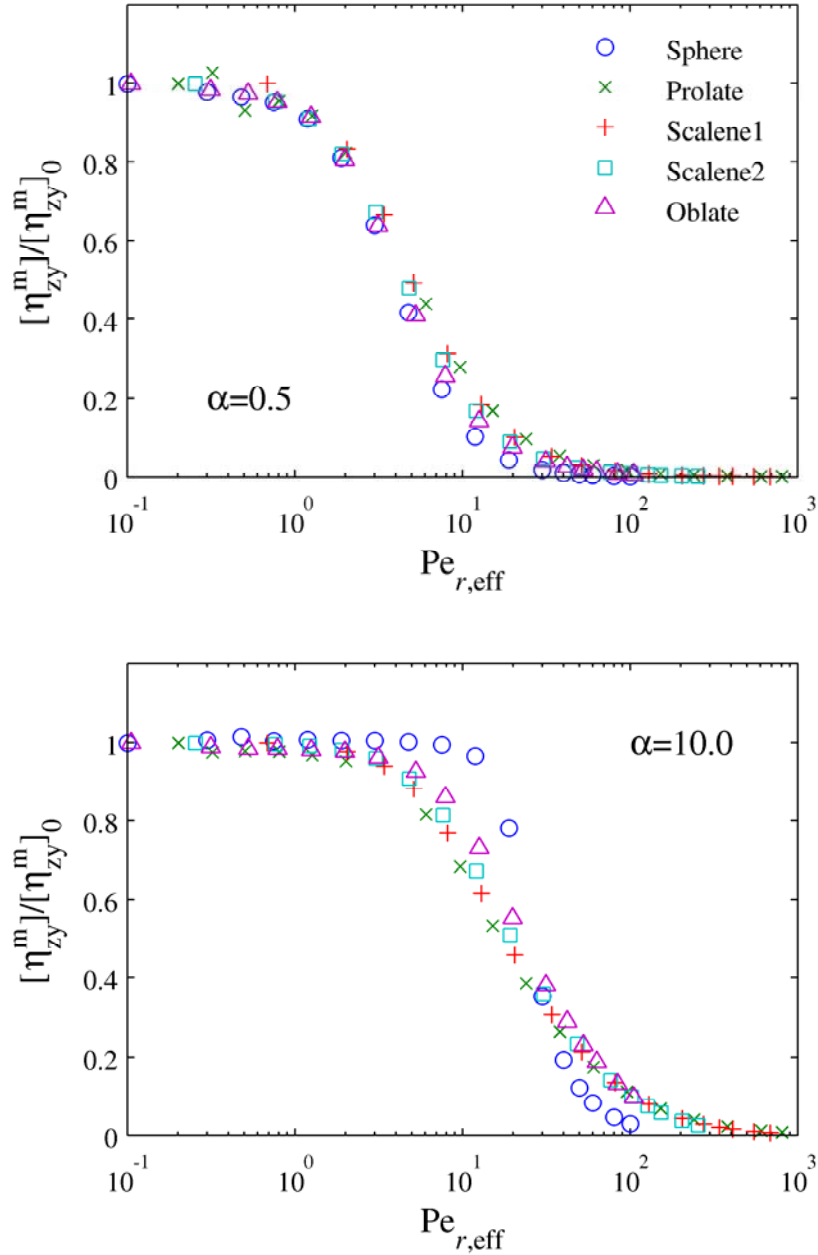


Figure 3-5: Normalized intrinsic magnetoviscosity as a function of $Pe_{r,eff}$ for different values of α . Here $[\eta_{zy}^m]_\infty$ is the intrinsic magnetoviscosity for $Pe_{r,eff} \rightarrow 0$.

It was found that there are two couples acting upon the particle: one tending to rotate the particle with the local vorticity of the fluid, and the other, from the rate-of-strain field, tending to turn the particle until its largest axis coincides with the principal direction of

Γ . Figure 3-6 confirms this fact, showing the orientational distribution of the magnetic dipole moment of different types of particles for $\alpha = 10$ and $Pe_{r,eff} = 18.93$.

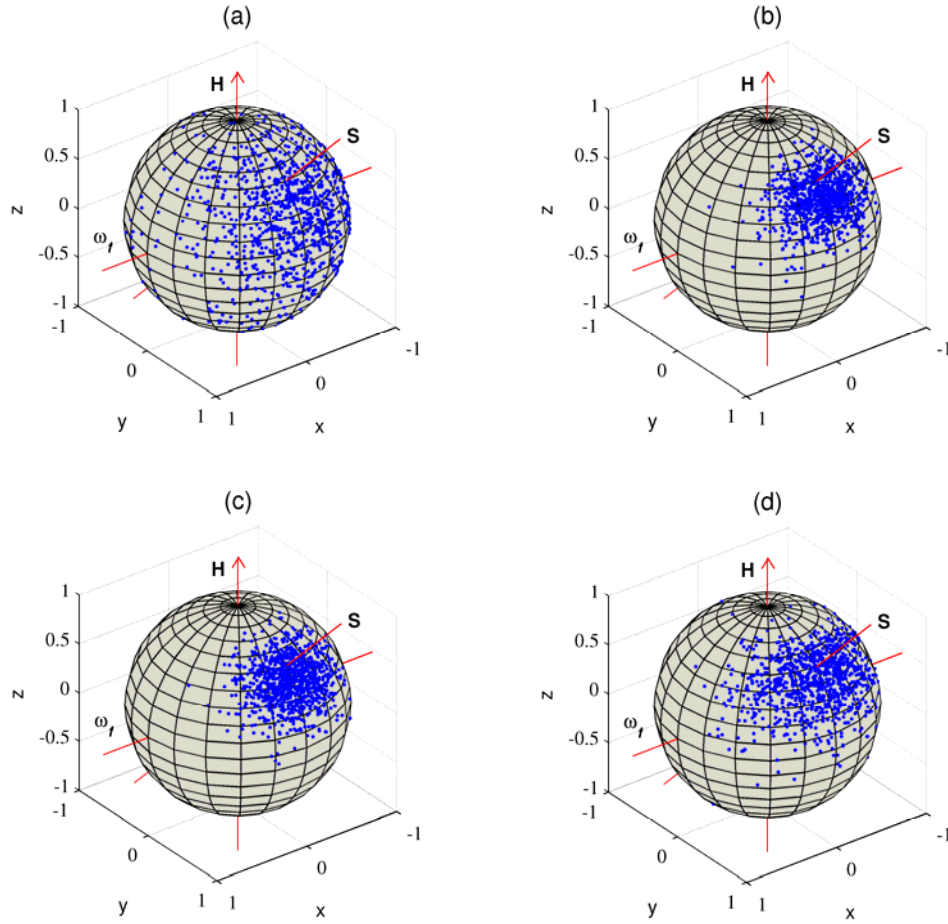


Figure 3-6: Orientational distribution of the magnetic dipole moment of (a) spherical particles, (b) prolate particles, (c) scalene particles, and (d) oblate particles, for $\alpha = 10$ and $Pe_{r,eff} = 18.93$. Dots correspond to particles with their magnetic dipole moments aligned with the corresponding point in the unit sphere. H arrow is the magnetic field direction, ω_f the angular velocity direction, and S the maximum strain direction.

For spherical particles the magnetic dipole moment distribution is almost isotropic on the upper half of the downstream hemisphere of orientation space due to the high shear rate and because the rate-of-strain field does not exert a torque on the spheres [67]. On

the other hand, the ellipsoidal particles tend to have their dipoles concentrated in the direction of maximum strain, resulting in a larger magnetic torque in (3.6).

3.4 Conclusions

Through rotational Brownian dynamics simulations we have studied the rheological properties, specifically magnetoviscosity, of dilute magnetic fluids composed of magnetized spherical and ellipsoidal particles in magnetic and shear flow fields. The governing equation of the infinitesimal rotation vector was derived from the stochastic angular momentum balance of a single particle and solved numerically. An intrinsic viscosity due to the magnetic field was calculated. The simulations have been carried out for a wide range of conditions in order to elucidate patterns in the behavior of these suspensions.

Results for spherical particles were compared with existing theoretical predictions and other numerical solutions. Good agreement was obtained with results from Brenner and Weissman [52] who studied the orientation distribution of dipolar Brownian spheres numerically. On the other hand, the intrinsic magnetoviscosity calculated from Shliomis' equation deviates from the results of the simulations for intermediate values of the Langevin parameter. Also, simulation results do not exhibit hysteresis of magnetoviscosity at high rotational Péclet numbers, as predicted by Shliomis [48] and He *et al.* [47]. These discrepancies are due to the use of an approximate phenomenological magnetization relaxation equation in their analyses.

Suspensions of ellipsoidal particles show a significant effect of aspect ratio on the intrinsic magnetoviscosity of the suspension. This effect is more significant as the aspect

ratio of the particles decreases. Thus, the intrinsic magnetoviscosity of suspensions of prolate particles saturates at lower α than oblate particles. Moreover, these kinds of suspensions also exhibit shear thinning behavior, with qualitative features that are in common with suspensions of spherical particles.

Using an effective rotational diffusion coefficient $D_{r,\text{eff}}$ it was possible to represent the normalized intrinsic magnetoviscosity as a unique function of Péclet number with α as a parameter. At high values of the Langevin parameter the results for magnetoviscosity of suspensions of spherical particles deviate from those for ellipsoidal particles. This discrepancy was attributed to the effect of the shear-torque on the orientation distribution of the non-spherical particles.

Because the possibility of magnetic control of the properties of magnetic fluids a wide variety of possible applications of these suspensions in different fields of engineering and biomedical can be developed. Thus for example, a magnetic fluid might be used to electronic control of the performance of damping systems such as clutches, brakes, and dampers.

4 MAGNETOVISCOSITY OF DILUTE MAGNETIC FLUIDS IN OSCILLATING AND ROTATING MAGNETIC FIELDS

The increase in the viscosity of a magnetic fluid under the influence of a constant magnetic field was discussed in Chapter 3 for suspensions of spherical and ellipsoidal particles. In this chapter, the effect of an alternating magnetic field on the rheological properties of magnetic fluids has been considered. In this case, under certain conditions the magnetic field reinforces the rotational motion of the particles and part of the energy of the magnetic field is transferred to the fluid as kinetic energy, accelerating the ferrofluid flow. This effect is seen as if the viscosity of the suspension decreased [68, 69]. Shliomis and Morozov [17] showed theoretically that if the magnetic field oscillates with a high enough frequency, $\Omega\tau_B > 1$, where Ω is the oscillating field frequency and τ_B is the Brownian relaxation time, the magnetoviscosity of a dilute suspension of spherical particles becomes negative. The expression derived by Shliomis and Morozov for the magnetoviscosity η^m in an oscillating magnetic field of small amplitude, was obtained solving the system of ferrohydrodynamic equations, which is given by

$$\eta^m = \frac{1}{4}\eta_0\phi\alpha^2 \frac{1 - \Omega^2\tau_B^2}{(1 + \Omega^2\tau_B^2)^2}, \quad (4.1)$$

where η_0 is the viscosity of the carrier fluid, ϕ is the volume fraction of particles, and α is the Langevin parameter, with μ_0 being the permeability of free space, μ the particle magnetic dipole, H the magnetic field, k_B Boltzmann's constant, and T the absolute temperature.

The so-called “negative viscosity effect” was first confirmed experimentally by Bacri *et al.*[7] for a water-based magnetic fluid composed of cobalt-ferrite (CoFe_2O_4) particles with a volume fraction of 20% and subjected to an oscillating magnetic field. A Poiseuille flow in a horizontal capillary tube was used for viscosity measurements. They observed a decrease of the magnetoviscosity to -19 cP at $H \sim 2000$ Oe and $\Omega \geq 700$ Hz .

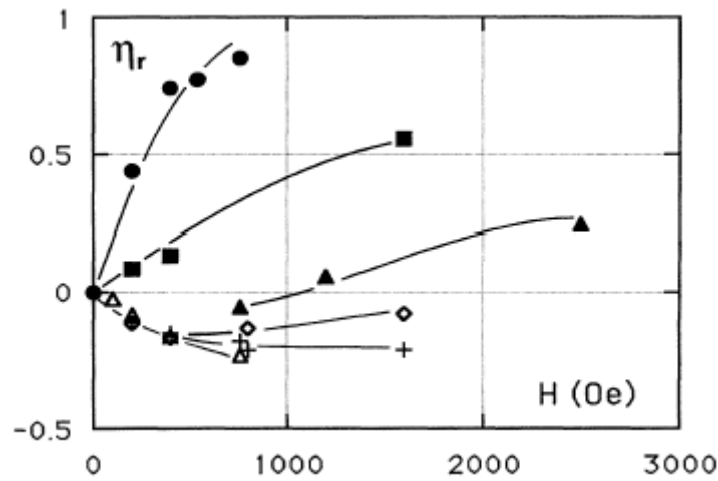


Figure 4-1: Experimental reduced viscosity $\eta_r = \eta^m / \eta$ versus magnetic field H for different frequencies f : ●: $f=0$; ■: $f=52$ Hz; ▲: $f=150$ Hz; ◇: $f=345$ Hz; +: $f=645$ Hz; △: $f=1480$ Hz. η is the viscosity of the suspension in zero magnetic field. Reproduced with permission from [70].

Later, Zeuner, Richter, and Rehberg [71], conducting an experiment similar to Bacri *et al.*, carried out a comparison of experimental results of reduced viscosity for a colloidal suspension of magnetite (Fe_3O_4) with the predictions of a theoretical model given in [7]

for finite values of α , which is based on the ferrohydrodynamics equations and the effective field method. They observed, for a large range of magnetic field strength and oscillation frequencies, the negative viscosity effect and found qualitative agreement between measurements and the theory given. The dependence of η^m on the flow vorticity in an oscillating magnetic field was studied experimentally by Gazeau *et al.* [72] for a ferrofluid in cylindrical Couette rheometer. They founded that the inner moving cylinder rotates at expense of the field for high field frequencies.

The effect of the flow vorticity was demonstrated theoretically by Krekov, Shliomis, and Kamiyama [69], who solved numerically a set of ferrohydrodynamic equations showing the non-Newtonian behavior of a dilute ferrofluid under conditions taking place in the experiments performed by Bacri *et al.* [7]. The calculations were performed with two different phenomenological magnetization equations in order to compare the results, employing the Eq. (3.15) and a magnetization equation derived from the Fokker-Planck equation. Their results show that Eq. (3.15) gives an adequate description of phenomenon in weak magnetic fields, and a nonlinear and nonmonotonic dependence of η^m on the flow vorticity. On the other hand, Morimoto, Maekawa, and Matsumoto [73] studied rheological and magnetic properties of a magnetic fluid composed of permanently magnetized spherical particles, subjected to both alternating magnetic and shear flow fields, by non-equilibrium Brownian dynamics simulations. The system was restricted to two dimensions (2D) and they took into account interparticle potentials such as dipole-dipole interactions, van der Waals attraction, and repulsion caused by surfactant contact. Their results show the effect on rotational viscosity of the magnetic field strength and shear rate for $Pe \geq 1$, exhibiting the negative viscosity effect, which was attributed to

resonance between the rotational motions of the particles and the fluctuation of the magnetic field.

The response of magnetic fluids to rotating magnetic fields was first observed experimentally by Moskowitz and Rosensweig [8] and studied theoretically by Zaitsev and Shliomis [74]. Interest here has centered on measurements of velocity profiles of concentrated suspensions since field rotation causes macroscopic motion of the fluid due to the average rotation of the suspended particles, a phenomenon known as spin-up flow [75]. On the other hand, the rheological properties of magnetic fluids subjected to rotating magnetic fields can be studied experimentally from measurements of the torque required to rotate a spindle submerged in ferrofluid. Thus, Rinaldi *et al.* [76] showed for a ferrofluid composed of magnetite particles that with the magnetic field counter-rotating and co-rotating with the spindle, the torque increases and decreases, respectively, as the strength of the magnetic field and frequency increase (see Figure 4-2). A decrease in the measured torque corresponds to a negative magnetoviscosity. In the experiments reported by Rinaldi *et al.* even negative torques can be measured, which would correspond to a negative effective viscosity of the suspension (that is, the magnetoviscosity is negative and larger in magnitude than the base fluid and Einstein viscosities). While there has been much work on the viscosity of magnetic fluids under oscillating magnetic fields, relatively few studies of the magnetoviscosity under rotating magnetic fields have been reported. Additionally, analytical models for magnetoviscosity in oscillating magnetic fields are based on the solution of the system of ferrohydrodynamic equations [7, 17, 77], which are limited by the assumptions of the magnetization relaxation equations used.

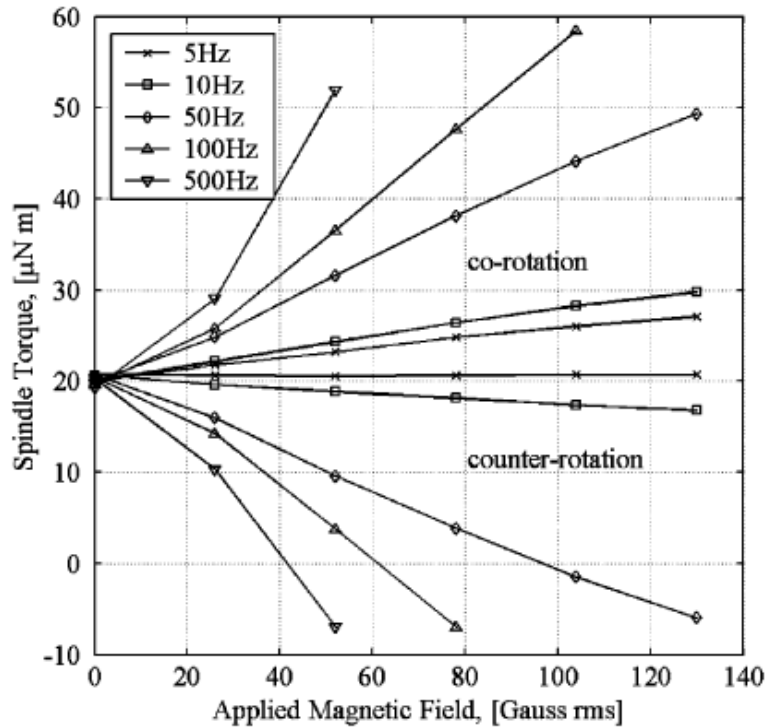


Figure 4-2: Torque required to rotate a spindle surrounded with ferrofluid at a rate of 100 rpm as function of applied field magnitude, rotation direction, and frequency. Reproduced with permission from [76].

In this chapter rotational Brownian dynamics simulations for the intrinsic magnetoviscosity $[\eta^m]$ of a magnetic fluid composed of non-interacting permanently magnetized spherical particles suspended in a Newtonian fluid and subjected to both magnetic fields and simple shear flow are presented. Furthermore, the effect of the amplitude and frequency of the external magnetic field and the magnitude of the shear rate on the intrinsic magnetoviscosity of the suspension was studied.

4.1 Calculation of the magnetoviscosity of the suspension

For the case of spherical particles (3.11) is given by

$$[\eta_{zy}^m] = -3 \frac{\alpha}{\text{Pe}_r} \left\langle \boldsymbol{\varepsilon} \cdot (\tilde{\boldsymbol{\mu}} \times \tilde{\mathbf{H}}) \right\rangle_{zy}. \quad (4.2)$$

Therefore, to calculate the time evolution of the intrinsic magnetoviscosity by numerical simulation it is necessary to express (4.2) in terms of the Euler parameters of the particles. Using the transformation matrix \mathbf{A} , the intrinsic magnetoviscosity of the suspension is then obtained from

$$[\eta_{zy}^m] = -3 \frac{\alpha}{\text{Pe}_r} \left\langle (e_0^2 - e_1^2 - e_2^2 + e_3^2) \tilde{H}_y - 2(e_2 e_3 - e_0 e_1) \tilde{H}_z \right\rangle. \quad (4.3)$$

Thus, from (4.3) in conjunction with (1.38) and (1.39), the evolution with time of the intrinsic magnetoviscosity is obtained.

4.2 Simulation parameters and conditions

The suspension was subjected to a simple shear flow as given by (1.21), and three types of simulation runs were performed: (i) response to an oscillating magnetic field $\tilde{\mathbf{H}} = \cos(\tilde{\Omega}\tilde{t})\mathbf{i}_z$, (ii) response to a co-rotating field $\tilde{\mathbf{H}} = \sin(\tilde{\Omega}\tilde{t})\mathbf{i}_y + \cos(\tilde{\Omega}\tilde{t})\mathbf{i}_z$, and (iii) response to a counter-rotating magnetic field $\tilde{\mathbf{H}} = \sin(\tilde{\Omega}\tilde{t})\mathbf{i}_y - \cos(\tilde{\Omega}\tilde{t})\mathbf{i}_z$. Here co-rotation means rotation in the same direction as the local vorticity of the fluid and counter-rotation in the opposite direction. All runs were performed starting from a random configuration, using 10^5 noninteracting spherical particles, a time step of $\Delta\tilde{t} = 0.01$, dimensionless frequency $\tilde{\Omega}$ in the range of 10^{-2} to 10^2 , and Langevin

parameters of $1 \leq \alpha \leq 10$. For a particle of typical size $d \sim 10$ nm suspended in a fluid with viscosity $\eta_0 \sim 10^{-3}$ Pa·s the Brownian relaxation time is very short $\tau_B \sim 10^{-7} - 10^{-6}$ s, therefore, large values of Péclet number are difficult to obtain in practice, so Pe_r was varied from 0.1 to 1.

4.3 Simulation results and discussion

The effect of the strength and frequency of an oscillating magnetic field on the intrinsic magnetoviscosity $[\eta_{zy}^m]$ is shown in Figure 4-3 for $Pe_r = 0.1$. At low frequency of the magnetic field the intrinsic magnetoviscosity approaches an equilibrium value, as shown in Chapter 3, and it decreases as the frequency increases. The intrinsic magnetoviscosity becomes negative at intermediate frequencies and will be zero at high frequencies, where the magnetic field has no effect on the magnetoviscosity. As showed numerically by Morimoto, Maekawa, and Matsumoto [73], at low magnetic field frequencies the angular velocity of the particles is lower than the angular velocity of the fluid, which results in an increase of the apparent viscosity. On the other hand, at higher frequencies the angular velocity of the particles is higher than the angular velocity of the fluid, which results in a decrease of the apparent viscosity, as mentioned in earlier. At very high frequencies the particles are unable to follow the magnetic field fluctuation and therefore the particles rotate freely with the local vorticity of the carrier fluid. Furthermore, Figure 4-3 shows that the minimum intrinsic magnetoviscosity decreases and the frequency corresponding to that minimum viscosity increases as the strength of the magnetic field, α , increases.

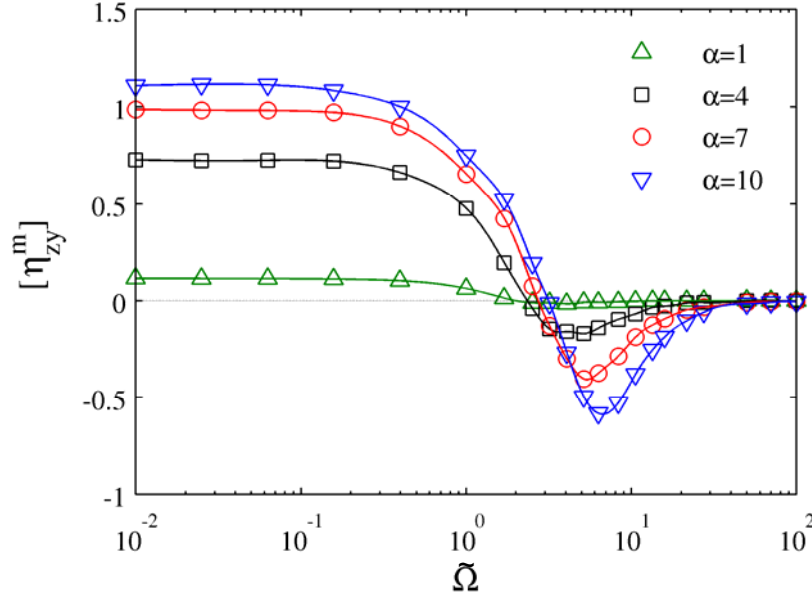


Figure 4-3: Dependence of the intrinsic magnetoviscosity on the magnitude and frequency of an oscillating magnetic field for $Pe_r = 0.1$.

On the other hand, rotating magnetic fields exhibit a dramatic effect on the apparent viscosity of the suspension. Figure 4-4 shows the effect of the amplitude and frequency of a rotating magnetic field on the intrinsic magnetoviscosity for $Pe_r = 0.1$. Results in Figure 4-4a show that when a co-rotating magnetic field is applied, the frequency of the magnetic field at which the intrinsic magnetoviscosity becomes zero is much lower in comparison with that of the alternating field case. Furthermore, the minimum value of the viscosity is much lower and its magnitude dramatically increases as the amplitude α of the magnetic field increases.

The field frequency required to reach the minimum intrinsic magnetoviscosity increases slightly as α increases. Also, the frequency range under which negative intrinsic magnetoviscosity appears is wider than for oscillating magnetic fields.

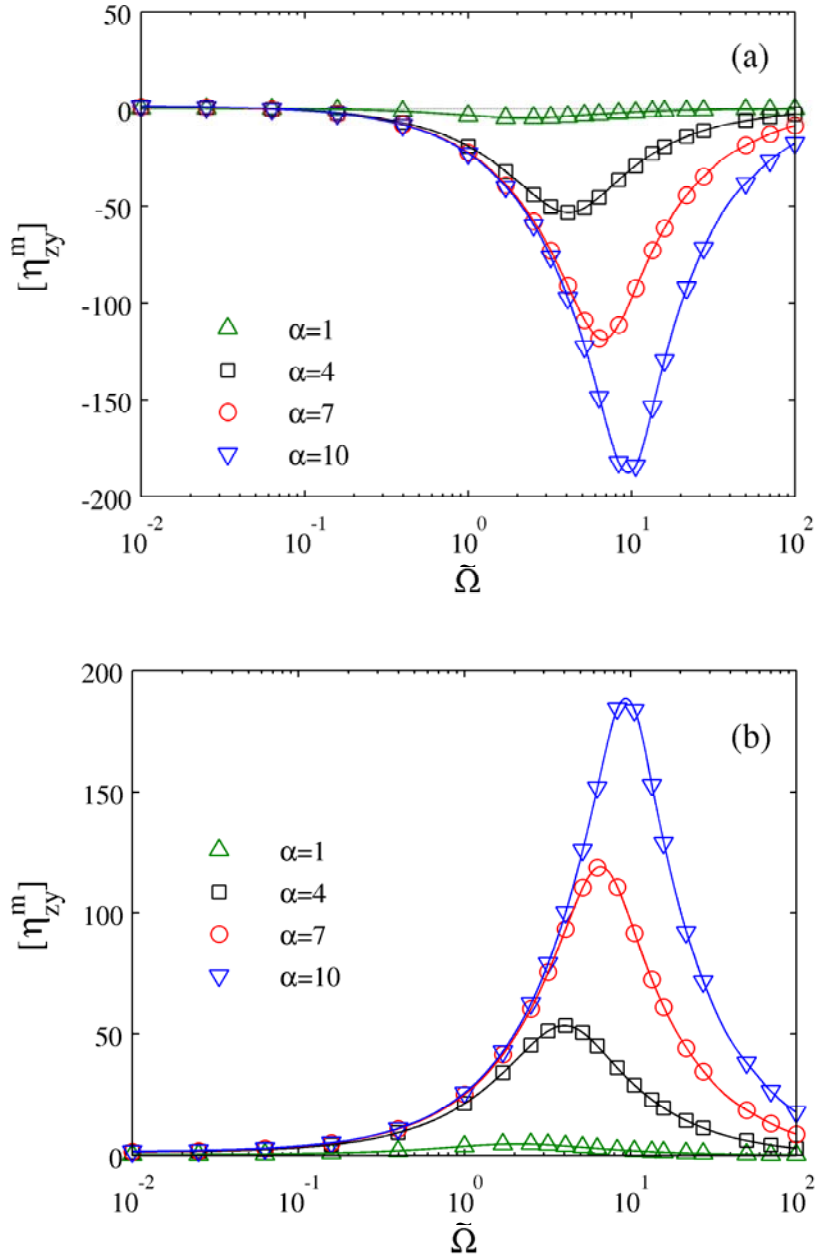


Figure 4-4: Dependence of the intrinsic magnetoviscosity on the magnitude and frequency of (a) a co-rotating and (b) a counter-rotating magnetic field for $Pe_r = 0.1$.

On the other hand, for a counter-rotating magnetic field, Figure 4-4b shows that the magnetoviscosity is always positive in the whole range of frequencies, exhibiting a peak of maximum magnetoviscosity which increases in magnitude as α increases. As for co-

rotating fields, the field frequency required to reach the maximum viscosity increases slightly as α increases.

It is important to note that the curve of intrinsic magnetoviscosity for counter-rotating field is almost a mirror image of that for co-rotating fields, which could be attributed to the fact that the particles are rotating in opposite direction, shifting thus the magnetoviscosity to positive values in the whole range of frequencies as seen from (4.6) and (4.7), and to the reversibility of the low Reynolds number flow [78] imposed on the particles.

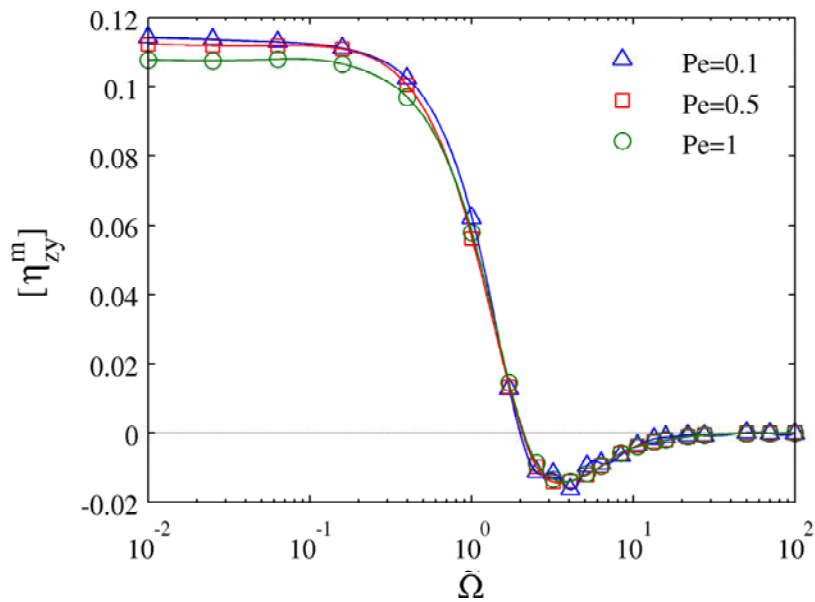


Figure 4-5: Dependence of the intrinsic magnetoviscosity on the Péclet number and frequency of an oscillating magnetic field for $\alpha = 1$.

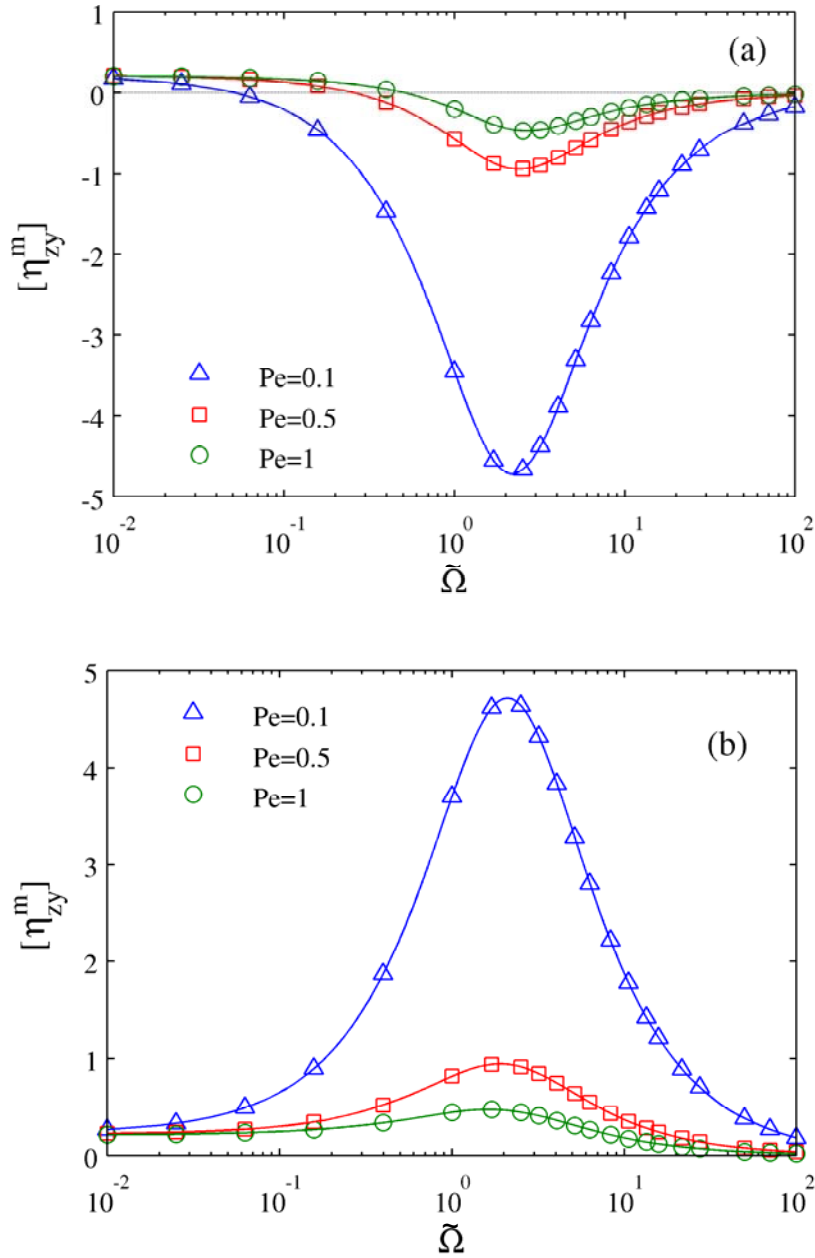


Figure 4-6: Dependence of the intrinsic magnetoviscosity on the Péclet number and frequency of (a) a co-rotating and (b) a counter-rotating magnetic field for $\alpha = 1$.

In contrast to the results obtained by Morimoto, Maekawa and Matsumoto [73] for $Pe_r = 1$ and 5, the Péclet number does not have a significant effect on the magnetoviscosity of the suspension in oscillating magnetic field for $0.1 \leq Pe_r \leq 1$, as

shown in Figure 4-5. On the other hand, under co-rotating magnetic fields, Figure 4-6a shows that, for $\alpha = 1$, the frequency where the intrinsic magnetoviscosity becomes zero is lower and the frequency range for negative viscosity is wider as Pe_r decreases. Furthermore, the field frequency required to reach the minimum intrinsic magnetoviscosity remains almost constant as Pe_r increases. The effect of the shear rate on the intrinsic magnetoviscosity in counter-rotating field shows behavior similar to that with a co-rotating magnetic field (see Figure 4-6b).

Figure 4-7 shows a comparison between the minimum values of the intrinsic magnetoviscosity obtained for both oscillating and co-rotating magnetic fields as a function of α and Pe_r . For both cases the figure shows that the magnitude of the intrinsic magnetoviscosity increases as the strength of the magnetic field increases.

In the simulated range the rotational Péclet number has no effect on $[\eta_{zy}^m]_{\min}$ for an oscillating magnetic field, Figure 4-7a; whereas in a co-rotating field, Figure 4-7b shows that the magnitude of $[\eta_{zy}^m]_{\min}$ increases as the Péclet number decreases. It is important to note that for $Pe_r = 0.1$ the magnitude of the minimum intrinsic magnetoviscosity for a co-rotating magnetic field is $\sim 10^2$ times greater than that for an oscillating magnetic field. Thus, the possibility to obtain negative values of the effective viscosity η_{eff} of a suspension composed of permanently magnetized spherical particles is attainable.

The effective viscosity of the suspension, subjected to an external magnetic field, can be obtained combining the symmetric and the antisymmetric parts of the viscous stress tensor. Therefore, from (3.4) and using the Eq. (1.19) and (3.10) we obtain

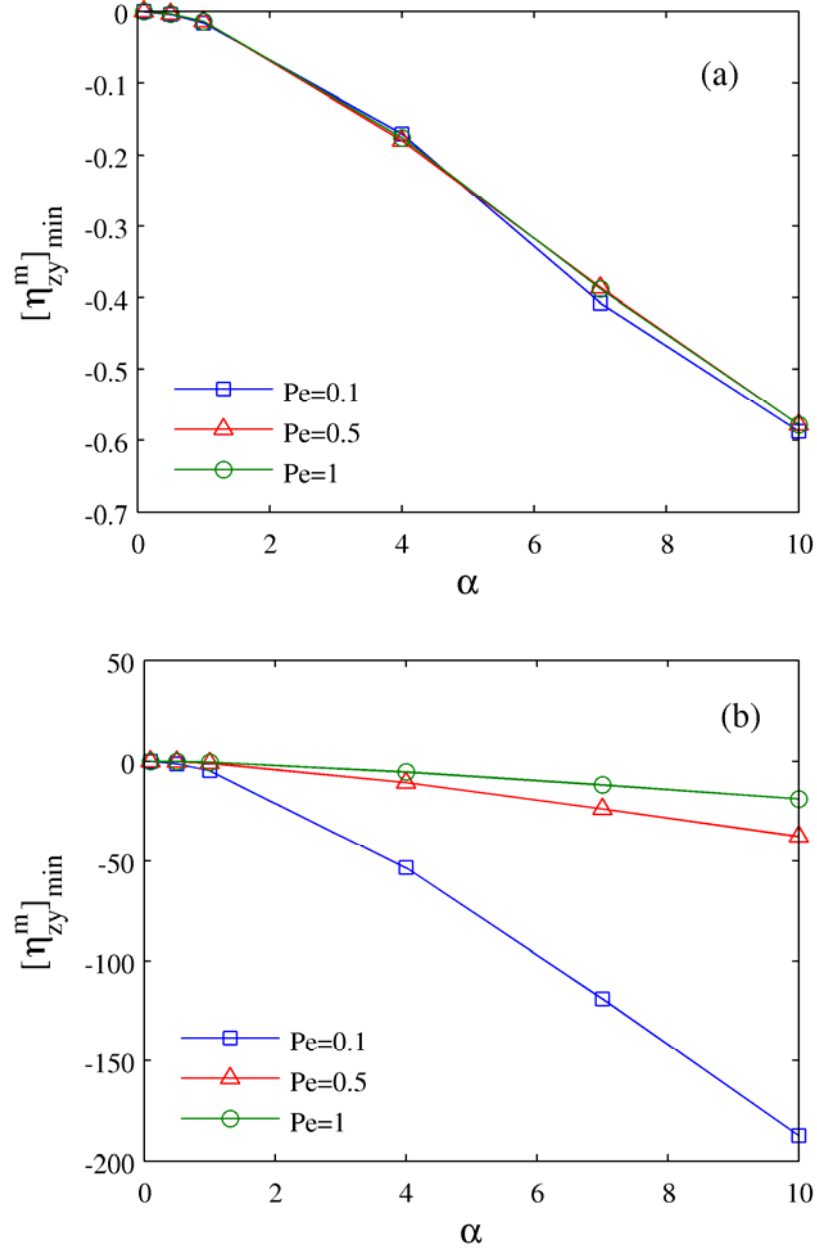


Figure 4-7: Minimum value of the intrinsic magnetoviscosity as a function of the Langevin parameter and Péclet number for (a) an oscillating and (b) a co-rotating magnetic field.

$$\tau_{zy} = \dot{\gamma} \eta_0 \left(1 + \frac{5}{2} \phi \right) + \dot{\gamma} \eta_0 \phi [\eta_{zy}^m]. \quad (4.4)$$

Thus, the effective viscosity of the suspension $\eta_{\text{eff}} = \tau_{zy} / \dot{\gamma}$ is then

$$\frac{\eta_{eff}}{\eta_0} = 1 + \phi \left(\frac{5}{2} + [\eta_{zy}^m] \right). \quad (4.5)$$

Equation (4.5) is plotted in Figure 4-8 as a function of the Langevin parameter for a particle volume fraction of $\phi = 0.01$, which we assume as a dilute enough suspension for the simulations to be representative. Figure 4-8 shows $\eta_{eff} < 0$ for high values of α and frequency under co-rotating magnetic field. This result is analogous to the torque measurements on commercial ferrofluid in rotating magnetic fields by Rinaldi *et al.* [76].

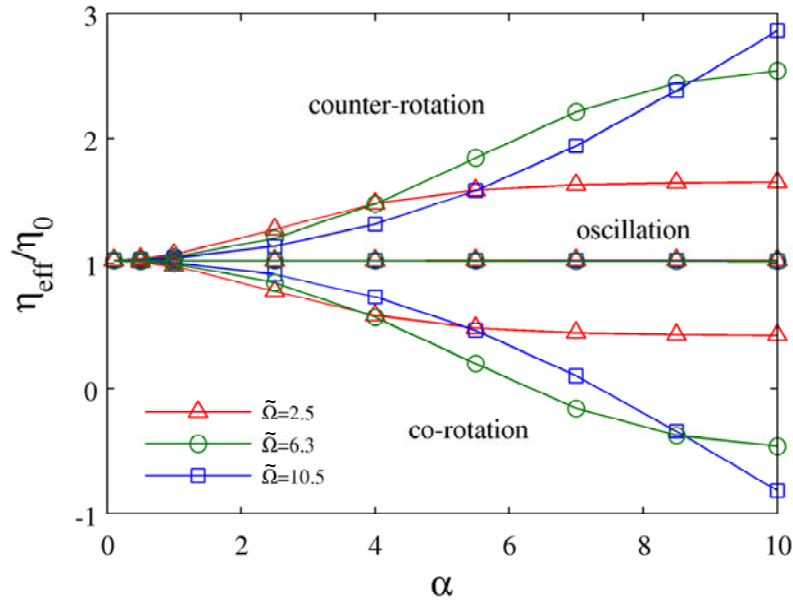


Figure 4-8: Normalized effective viscosity of the suspension as a function of the Langevin parameter for $Pe_r = 0.1$ and $\phi = 0.01$.

According to this, the fluid behaves as if it is filled with nanosized rotors that reduce the friction between adjacent fluid layers [72] due to the transfer of part of the magnetic field energy as kinetic energy into the fluid, leading to a decrease in the

effective viscosity of the suspension. Figure 4-8 also shows a negligible effect of the oscillating magnetic field on η_{eff} in comparison with the case of rotating magnetic fields.

In the negative intrinsic magnetoviscosity regions, the mean angular velocity of the particles should be higher than the local angular velocity of the carrier fluid. To illustrate this, we determined the dimensionless mean angular velocity of the particles $\langle \tilde{\omega}_x \rangle$ and compared it with the local angular velocity of the carrier fluid $\tilde{\omega}_f = 1/2$. The time variation of the mean angular displacement $\langle \tilde{\Phi}_x(\tilde{t}) \rangle$ about the x -axis is shown in Figure 4-9 for $\alpha = 4$ and $Pe_r = 1$. Note that the slope in Figure 4-9 gives the dimensionless mean angular velocity of the particles.

In the case of a co-rotating magnetic field, Figure 4-9a shows for $\tilde{\Omega} = 0.1$ that the mean angular velocity of the particles is lower than the fluid angular velocity, $|\langle \tilde{\omega}_x \rangle| < \tilde{\omega}_f$, which leads to positive values of the intrinsic magnetoviscosity. As the field frequency increases, the mean angular velocity of the particles eventually is higher than the angular velocity of the fluid, $|\langle \tilde{\omega}_x \rangle| > \tilde{\omega}_f$, and the magnetoviscosity becomes negative. At very high magnetic field frequencies the particles cannot follow the magnetic field rotation, therefore they rotate freely with the fluid, $|\langle \tilde{\omega}_x \rangle| = \tilde{\omega}_f$, and the suspension behaves as a torque-free suspension. Whence, the effect of the rotating magnetic field on the intrinsic magnetoviscosity disappears.

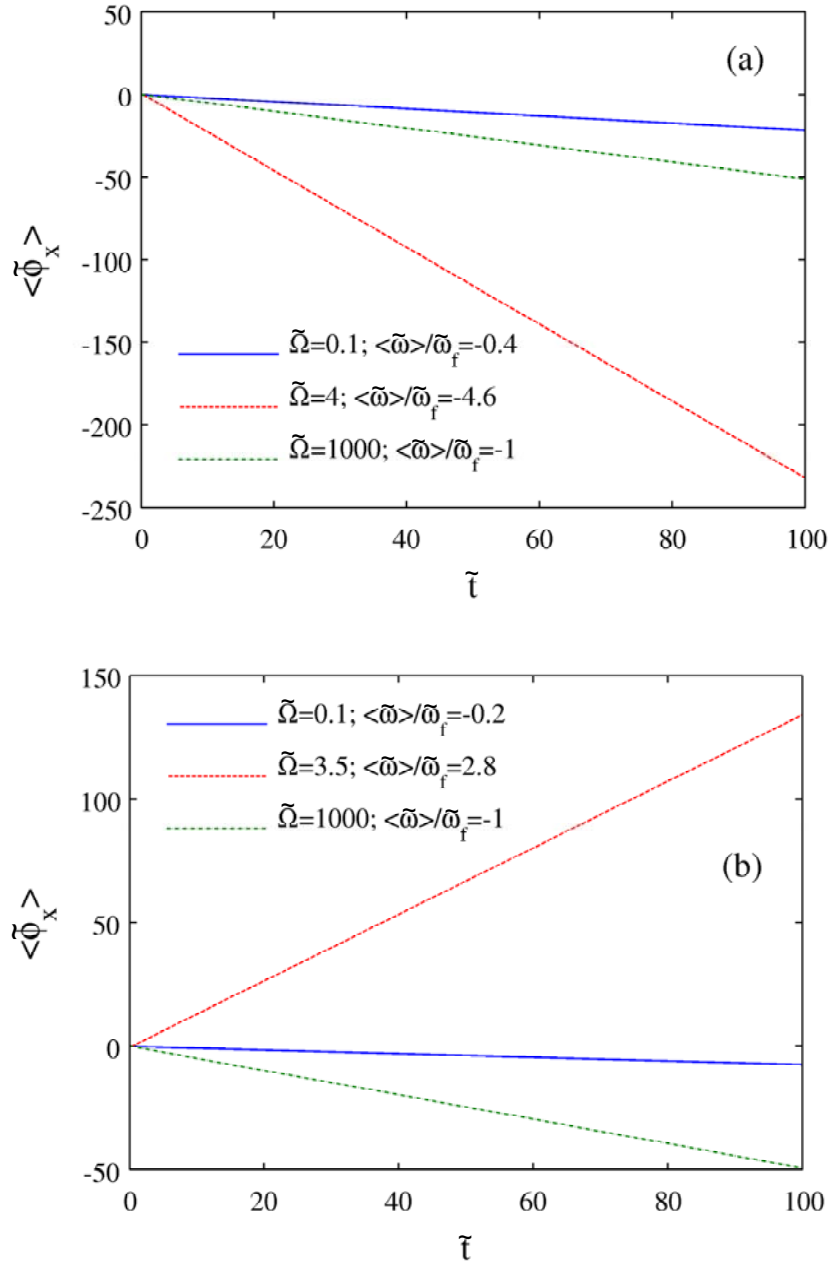


Figure 4-9: Time variation of the mean angular displacement of magnetic particles in both (a) co-rotating and (b) counter-rotating magnetic fields for $\alpha = 4$ and $Pe_\gamma = 1$.

In the case of a counter-rotating magnetic field, Figure 4-9b shows that for $\tilde{\Omega} = 0.1$ the particles rotate slower than in the case of a co-rotating field in the same direction as the local vorticity, which is because the hydrodynamic torque dominates the magnetic

torque. As the frequency increases, the magnetic torque dominates and the particles rotate in opposite direction to the local vorticity, therefore the intrinsic magnetoviscosity increases. At very high frequencies the magnetic field has no effect on $[\eta_{zy}^m]$.

The results shown in Figure 4-9a qualitatively agree with those obtained by Morimoto, Maekawa and Matsumoto [73] for oscillating magnetic fields, showing an increase of the average angular velocity of the particles relative to that for oscillating field.

We compared the dimensionless mean angular velocity of the particles for $\alpha = 1$ and $Pe_r = 1$, when they are subjected to oscillating and co-rotating magnetic fields. Figure 4-10 shows that for $\tilde{\Omega} = 2.5$, in an oscillating magnetic field the particles rotate at the same angular velocity of the fluid, but in a co-rotating magnetic field the particles rotate faster than the fluid, which leads to lower values in the negative intrinsic magnetoviscosity.

The reason for the discrepancy in the angular velocity of the particles is that, as shown in Figure 4-11, for an oscillating magnetic field the magnetic torque changes direction as the particles rotate and the field oscillates, at times reducing the rotation rate of the particles; whereas for a co-rotating magnetic field the magnetic torque always reinforces the rotation in the same direction of the local vorticity, increasing the rotation rate of the particles.

The results from these simulations can also be used to verify the suspension scale constitutive equation governing the antisymmetric part of the deviatoric stress, which according to Condiff and Dahler [61] is given by

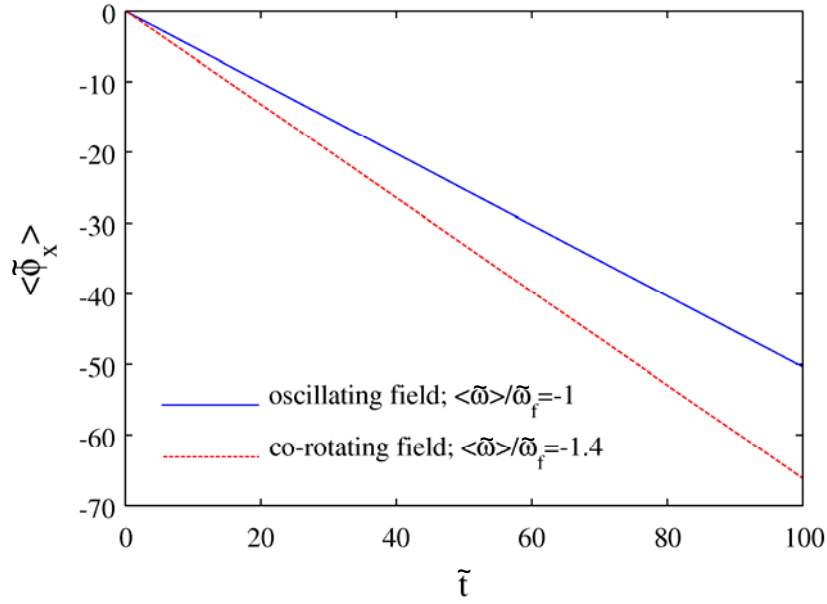


Figure 4-10: Comparison of variations of the mean angular displacement of magnetic particles in oscillating and co-rotating magnetic fields at $\tilde{\Omega} = 2.5$ for $\alpha = 1$ and $Pe_r = 1$.

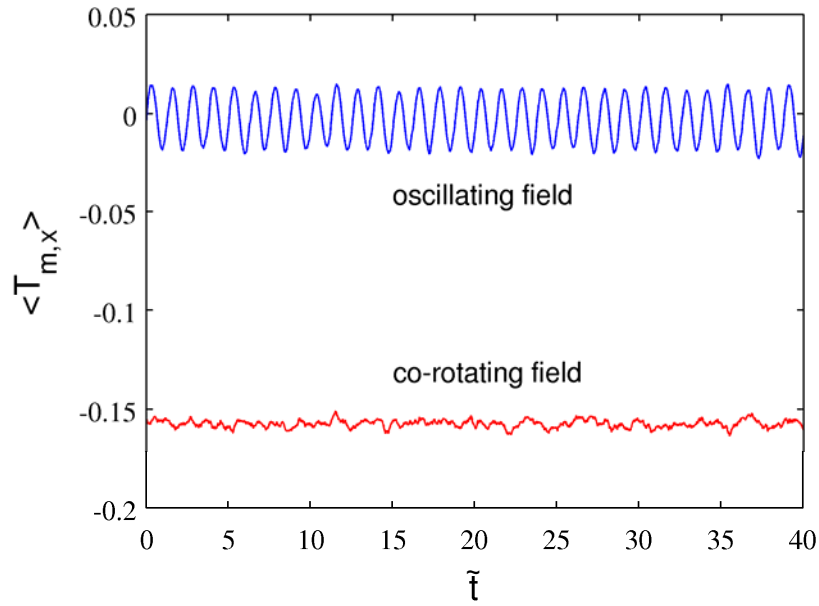


Figure 4-11: Variation of the macroscopic magnetic torque ($\langle \mathbf{T} \rangle = \tilde{\mathbf{m}} \times \tilde{\mathbf{H}}$, where $\tilde{\mathbf{m}}$ is the dimensionless magnetization of the suspension) in the flow vorticity direction (x -axis) with time in an oscillating and a co-rotating magnetic field at $\tilde{\Omega} = 2.5$ for $\alpha = 1$ and $Pe_r = 1$.

$$\boldsymbol{\tau}^a = \frac{1}{2} \eta_v \boldsymbol{\varepsilon} \cdot \left[\left(\frac{1}{2} \right) \nabla \times \mathbf{v} - \langle \boldsymbol{\omega} \rangle \right]. \quad (4.6)$$

Here $\eta_v = 6\eta_0\phi$ is the vortex viscosity [64] and $\langle \boldsymbol{\omega} \rangle$ is the average angular velocity of the particulate phase of the suspension. Combining (1.21), (1.37), (3.10), and (4.6) it is obtained, in dimensionless form, that

$$[\eta_{zy}^m] = 3 \left(\frac{1}{2} + \frac{\langle \tilde{\omega}_x \rangle}{\text{Pe}} \right). \quad (4.7)$$

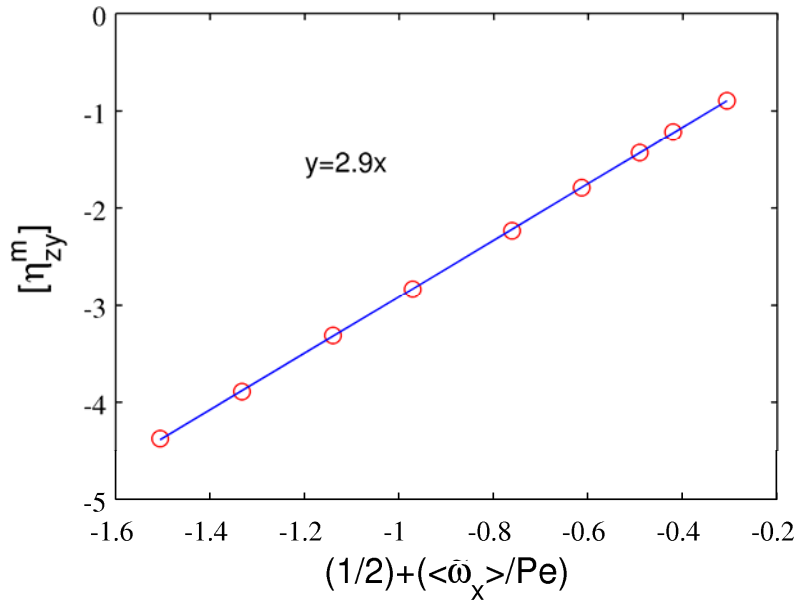


Figure 4-12: Intrinsic magnetoviscosity in co-rotating magnetic field as function of the angular slip velocity for $\alpha = 1$ and $\text{Pe}_r = 0.1$.

Figure 4-12 clearly demonstrates that the intrinsic magnetoviscosity obtained by Brownian dynamics simulation agrees well with the theoretical prediction for dilute

suspensions given by (4.7); whence, this result confirms the correctness of the constitutive equation (4.6) for the antisymmetric stress. A similar result was obtained by Feng *et al.* [62] by numerical boundary element method simulations but neglecting particle Brownian motion.

4.4 Conclusions

Using rotational Brownian dynamics simulations, the rheological properties, specifically intrinsic magnetoviscosity, of dilute magnetic fluids composed of magnetized spherical particles in oscillating/rotating magnetic fields and simple shear flow were studied. The governing equation of the infinitesimal rotation vector was derived from the stochastic angular momentum balance of a single particle and solved numerically. An intrinsic viscosity due to the magnetic field was calculated. The simulations have been carried out for a wide range of conditions in order to compare the effect of alternating and rotating magnetic fields.

Results for oscillating magnetic field are in agreement with those obtained in [73], showing additionally that the Péclet number does not have a significant effect on the magnetoviscosity for $Pe_r \leq 1$. Simulation results show a considerable effect of a co-rotating magnetic field on the intrinsic magnetoviscosity in comparison with an oscillating magnetic field. Indeed, compared to oscillating magnetic fields, for co-rotating fields the intrinsic magnetoviscosity becomes zero at lower frequency and the minimum viscosity obtained is much lower at the same values of α and Pe_r parameters. In counter-rotating magnetic fields the intrinsic magnetoviscosity was positive in the whole range of field amplitude and frequency and exhibits a maximum at an intermediate

frequency. In this case the particles rotate slower or in opposite direction to the local angular velocity of the fluid. In the negative intrinsic magnetoviscosity regions, the mean angular velocity of the particles is higher than the local angular velocity of the fluid. In co-rotating magnetic fields particles rotate faster than in oscillating magnetic fields, which results in higher magnitude of negative magnetoviscosity. Therefore, co-rotating magnetic fields seem to be suitable to obtain negative effective viscosity in magnetic nanoparticles suspensions. Finally, simulation results for the intrinsic magnetoviscosity show that the commonly accepted constitutive equation for the antisymmetric part of the viscous stress tensor is applicable to dilute suspensions of spherical particles.

As has been discussed in previous chapters, the magnetic field exerts a torque to the magnetic particles in the suspension, influencing their free rotation in a shear flow, thus changing the viscosity of the suspension even to negative values. This attractive property could lead to a new generation of adaptive dampers. As a consequence, experiments to provide a quantitative proof of the above mentioned numerical approaches have to be performed. However, an investigation of magnetoviscous effects in magnetic fluids does not only require the possibility of application of variable magnetic fields and shear rate, but also make use of suspensions composed of asymmetric particles. This can be done by a modification of commercially available rheometers and by desing of the particle's geometry.

BIBLIOGRAPHY

- [1] R. E. Rosensweig, *Ferrohydrodynamics* (Cambridge University Press, New York, 1985).
- [2] S. Odenbach, *Magnetoviscous effects in ferrofluids* (Springer, Berlin, 2002).
- [3] S. Odenbach, "Ferrofluids--magnetically controlled suspensions," *Colloids and Surfaces A: Physicochemical and Engineering Aspects*, Vol. **217**, pp 171 (2003).
- [4] C. Rinaldi, A. Chaves, S. Elborai, X. T. He, and M. Zahn, "Magnetic fluid rheology and flows," *Current Opinion in Colloid & Interface Science*, Vol. **10**, pp 141 (2005).
- [5] J. P. McTague, "Magnetoviscosity of magnetic colloids," *Journal of Chemical Physics*, Vol. **51**, pp 133 (1969).
- [6] R. E. Rosensweig, R. Kaiser, and G. Miskolczy, "Viscosity of magnetic fluid in a magnetic field," *Journal of Colloid and Interface Science*, Vol. **29**, pp 680 (1969).
- [7] J. C. Bacri, R. Perzynski, M. I. Shliomis, and G. I. Burde, ""Negative-viscosity" effect in a magnetic fluid," *Physical Review Letters*, Vol. **75**, pp 2128 (1995).
- [8] R. Moskowitz, and R. E. Rosensweig, "Nonmechanical torque-driven flow of a ferromagnetic fluid by an electromagnetic field," *Applied Physics Letters*, Vol. **11**, pp 301 (1967).
- [9] R. Mazo, *Brownian Motion: Fluctuations, Dynamics and Applications* (Oxford University Press, New York, 2002).
- [10] P. C. Fannin, B. K. P. Scaife, A. T. Giannitsis, and S. W. Charles, "Determination of the radius of nano-particles in a magnetic fluid by means of a constant frequency measurement technique," *Journal of Physics D: Applied Physics*, Vol. **35**, pp 1305 (2002).
- [11] P. C. Fannin, "Investigating magnetic fluids by means of complex susceptibility measurements," *Journal of Magnetism and Magnetic Materials*, Vol. **258-259**, pp 446 (2003).
- [12] P. C. Fannin, "Characterisation of magnetic fluids," *Journal of Alloys and Compounds*, Vol. **369**, pp 43 (2004).

- [13] V. L. Calero-DdelC, C. Rinaldi, and M. Zahn, "Magnetic fluids and nanoparticle based sensors," in *Encyclopedia of Sensors*, Vol 5, edited by C. A. Grimes, E. C. Dickey and M. V. Pishko (American Scientific Publishers, 2006), pp. 389.
- [14] A. Einstein, "Eine neue bestimmung der molekuldimensionen," *Annalen der Physik*, Vol. **324**, pp 289 (1906).
- [15] W. M. Deen, *Analysis of transport phenomena* (Oxford University Press, New York, 1998).
- [16] P. Rajinder, *Rheology of particulate dispersions and composites* (CRC Press, Boca Raton, 2007).
- [17] M. I. Shliomis, and K. I. Morozov, "Negative viscosity of ferrofluid under alternating magnetic field," *Physics of Fluids*, Vol. **6**, pp 2855 (1994).
- [18] H. C. Otinger, *Stochastic processes in polymeric fluids. Tools and examples for developing simulation algorithms.* (Springer, Berlin, 1996).
- [19] J. Happel, and H. Brenner, *Low Reynolds number hydrodynamics* (Prentice-Hall, Englewood Cliffs, 1965).
- [20] H. Brenner, "The Stokes resistance of an arbitrary particle-III: Shear fields," *Chemical Engineering Science*, Vol. **19**, pp 631 (1964).
- [21] C. Rinaldi, "An invariant general solution for the magnetic fields within and surrounding a small spherical particle in an imposed arbitrary magnetic field and the resulting magnetic force and couple," *Chemical Engineering Communications*, Vol. **197**, pp 92 (2010).
- [22] H. Goldstein, C. Poole, and J. Safko, *Classical Mechanics* (Addison Wesley, San Francisco, 2002).
- [23] E. Dickinson, "Brownian dynamics with rotation-translation coupling," *Journal of the Chemical Society, Faraday Transactions 2*, Vol. **81**, pp 591 (1985).
- [24] D. Mukhija, and M. J. Solomon, "Translational and rotational dynamics of colloidal rods by direct visualization with confocal microscopy," *Journal of Colloid and Interface Science*, Vol. **314**, pp 98 (2007).
- [25] M. I. Mishchenko, "Electromagnetic scattering by nonspherical particles: A tutorial review," *Journal of Quantitative Spectroscopy and Radiative Transfer*, Vol. **110**, pp 808 (2009).

- [26] S. H. Lee, and C. M. Liddell, "Anisotropic magnetic colloids: A strategy to form complex structures using nonspherical building blocks," *Small*, Vol. **5**, pp 1957 (2009).
- [27] A. Satoh, "Rheological properties and orientational distributions of dilute ferromagnetic spherocylinder particle dispersions," *Journal of Colloid and Interface Science*, Vol. **234**, pp 425 (2001).
- [28] Y. L. Raikher, and V. Rusakov, "On the solution of the Fokker-Planck equation for dipolar particles in a viscoelastic fluid," *Journal of Molecular Liquids*, Vol. **71**, pp 81 (1997).
- [29] Y. L. Raikher, and V. Rusakov, "Dynamic of magneto-orientational susceptibility in a viscoelastic magnetic fluid," *Journal of Magnetism and Magnetic Materials*, Vol. **201**, pp 201 (1999).
- [30] V. S. Volkov, and A. I. Leonov, "Rotational Brownian motion of axisymmetric particles in a Maxwell fluid," *Physical Review E*, Vol. **64**, pp 051113 (2001).
- [31] D. L. Ermak, and J. A. McCammon, "Brownian dynamics with hydrodynamics interactions," *Journal of Chemical Physics*, Vol. **69**, pp 1352 (1978).
- [32] G. Meriguet, M. Jardat, and P. Turq, "Brownian dynamics investigation of magnetization and birefringence relaxations in ferrofluids," *Journal of Chemical Physics*, Vol. **123**, pp 144915 (2005).
- [33] A. Satoh, "Influence of magnetic interactions between clusters on particle orientational characteristics and viscosity of a colloidal dispersion composed of ferromagnetic spherocylinder particles: Analysis by means of mean field approximation for a simple shear flow," *Journal of Colloid and Interface Science*, Vol. **289**, pp 276 (2005).
- [34] Y. Han, A. M. Alsayed, M. Nobili, J. Zhang, T. C. Lubensky, and A. G. Yodh, "Brownian motion of an ellipsoid," *Science*, Vol. **314**, pp 626 (2006).
- [35] C. Scherer, and H. G. Matuttis, "Rotational dynamics of magnetic particles in suspension," *Physical Review E*, Vol. **63**, pp 011504 (2000).
- [36] F. Perrin, "Mouvement Brownien d'un ellipsoide (I). Dispersion dielectrique pour des molecules ellipsoidales," *Le Journal de Physique et le Radium*, Vol. **5**, pp 497 (1934).

- [37] W. T. Coffey, Y. P. Kalmykov, and J. T. Waldron, *The Langevin equation: with applications to stochastic problems in physics, chemistry and electrical engineering* (World Scientific, Singapore, 2004).
- [38] S. Morita, and H. Ushiki, "Rotational behavior of the fluorescent probe molecules near the critical point of phase separation," *Physica B: Condensed Matter*, Vol. **327**, pp 108 (2003).
- [39] M. L. Barcellona, and E. Gratton, "Fluorescence anisotropy of DNA/DAPI complex: torsional dynamics and geometry of the complex," *Biophysical Journal*, Vol. **70**, pp 2341 (1996).
- [40] E. W. Small, and I. Isenberg, "Hydrodynamic properties of a rigid molecule: Rotational and linear diffusion and fluorescence anisotropy," *Biopolymers*, Vol. **16**, pp 1907 (1977).
- [41] G. Weber, "Theory of Fluorescence Depolarization by Anisotropic Brownian Rotations. Discontinuous Distribution Approach," *Journal of Chemical Physics*, Vol. **55**, pp 2399 (1971).
- [42] T. J. Chuang, and K. B. Eisenthal, "Theory of Fluorescence Depolarization by Anisotropic Rotational Diffusion," *Journal of Chemical Physics*, Vol. **57**, pp 5094 (1972).
- [43] M. Ehrenberg, and R. Rigler, "Polarized fluorescence and rotational Brownian motion," *Chemical Physics letters*, Vol. **14**, pp 539 (1972).
- [44] Y. P. Kalmykov, and S. V. Titov, "Anisotropic rotational diffusion and transient nonlinear responses of rigid macromolecules in a strong external electric field," *Journal of Chemical Physics*, Vol. **126**, pp 174903 (2007).
- [45] Y. P. Kalmykov, and S. V. Titov, "Anisotropic rotational diffusion and dielectric relaxation of rigid dipolar particles in a strong external dc field," *Physical Review E*, Vol. **78**, pp 051110 (2008).
- [46] A. Bruno, M. Alfè, B. Apicella, C. de Lisio, and P. Minutolo, "Characterization of nanometric carbon materials by time-resolved fluorescence polarization anisotropy," *Optics and Lasers in Engineering*, Vol. **44**, pp 732 (2006).
- [47] X. He, S. Elborai, D. Kim, S. Lee, and M. Zahn, "Effective magnetoviscosity of planar-Couette magnetic fluid flow," *Journal of Applied Physics*, Vol. **97**, pp 10Q302 (2005).

- [48] M. I. Shliomis, "Effective viscosity of magnetic suspensions," *Soviet Physics JETP*, Vol. **34**, pp 1291 (1972).
- [49] A. Einstein, "Berichtigung zu meiner arbeit: "Eine neue bestimmung der molekuldimensionen"," *Annalen der Physik*, Vol. **339**, pp 591 (1911).
- [50] W. F. Hall, and S. N. Busenberg, "Viscosity of magnetic suspensions," *Journal of Chemical Physics*, Vol. **51**, pp 137 (1969).
- [51] M. I. Shliomis, "Ferrohydrodynamics: Testing a third magnetization equation," *Physical Review E*, Vol. **64**, pp 060501 (2001).
- [52] H. Brenner, and M. H. Weissman, "Rheology of a dilute suspension of dipolar spherical particles in an external field. II. Effects of rotary Brownian motion," *Journal of Colloid and Interface Science*, Vol. **41**, pp 499 (1972).
- [53] S. Yamamoto, and T. Matsuoka, "A method for dynamic simulation of rigid and flexible fibers in a flow field," *Journal of Chemical Physics*, Vol. **98**, pp 644 (1993).
- [54] K. Asokan, and T. R. Ramamohan, "The rheology of a dilute suspension of Brownian dipolar spheroids in a simple shear flow under the action of an external force," *Physics of Fluids*, Vol. **16**, pp 433 (2004).
- [55] P. S. Doyle, and E. S. Shaqfeh, "Dynamic simulation of freely-draining, flexible bead-rod chains: Start-up of extensional and shear flow," *Journal of Non-Newtonian Fluid Mechanics*, Vol. **76**, pp 43 (1998).
- [56] A. Hijazi, and M. Zoaeter, "Brownian dynamics simulation for rod-like particles in dilute flowing solutions," *European Polymer Journal*, Vol. **38**, pp 2207 (2002).
- [57] C. Salueña, A. Pérez-Madrid, and J. M. Rubí, "The viscosity of a suspension of ferromagnetic rod-like particles," *Journal of Colloid and Interface Science*, Vol. **164**, pp 269 (1994).
- [58] S. R. Strand, and S. Kim, "Dynamics and rheology of a dilute suspension of dipolar nonspherical particles in an external field: Part 1. Steady shear flows.," *Rheologica Acta*, Vol. **31**, pp 94 (1992).
- [59] A. Satoh, and M. Ozaki, "Transport coefficients and orientational distributions of spherical particles with magnetic moment normal to the particle axis (analysis for an applied magnetic field normal to the shear plane)," *Journal of Colloid and Interface Science*, Vol. **298**, pp 957 (2006).

- [60] A. Satoh, M. Ozaki, T. Ishikawa, and T. Majima, "Transport coefficients and orientational distributions of rodlike particles with magnetic moment normal to the particle axis under circumstances of a simple shear flow," *Journal of Colloid and Interface Science*, Vol. **292**, pp 581 (2005).
- [61] D. W. Condiff, and J. S. Dahler, "Fluid mechanical aspects of antisymmetric stress," *Physics of Fluids*, Vol. **7**, pp 842 (1964).
- [62] S. Feng, A. L. Graham, J. R. Abbott, and H. Brenner, "Antisymmetric stresses in suspensions: vortex viscosity and energy dissipation," *Journal of Fluid Mechanics*, Vol. **563**, pp 97 (2006).
- [63] H. Brenner, "Rheology of a dilute suspension of dipolar spherical particles in an external field," *Journal of Colloid and Interface Science*, Vol. **32**, pp 141 (1970).
- [64] H. Brenner, "Rheology of two-phase systems," *Annual review of fluid mechanics*, Vol. **2**, pp 137 (1970).
- [65] H. Brenner, "The Stokes resistance of an arbitrary particle - II," *Chemical Engineering Science*, Vol. **19**, pp 599 (1964).
- [66] G. B. Jeffery, "The motion of ellipsoidal particles immersed in a viscous fluid," *Proceedings of the Royal Society A*, Vol. **102**, pp 161 (1922).
- [67] G. K. Batchelor, "The stress system in a suspension of force-free particles," *Journal of Fluid Mechanics*, Vol. **41**, pp 545 (1970).
- [68] C. Rinaldi, T. Franklin, M. Zahn, and T. Cader, "Magnetic nanoparticles in fluid suspension: Ferrofluid applications," in *Encyclopedia of Nanoscience and Nanotechnology*, Vol edited by (Marcel Dekker, Inc., 2004), pp. 1.
- [69] A. P. Krekhov, M. I. Shliomis, and S. Kamiyama, "Ferrofluid pipe flow in an oscillating magnetic field," *Physics of Fluids*, Vol. **17**, pp 033105 (2005).
- [70] J. C. Bacri, R. Perzynski, M. I. Shliomis, and G. I. Burde, ""Negative-viscosity" effect in a magnetic fluid," *Phys. Rev. Lett.*, Vol. **75**, pp 2128 (1995).
- [71] A. Zeuner, R. Richter, and I. Rehberg, "Experiments on negative and positive magnetoviscosity in an alternating magnetic field," *Physical Review E*, Vol. **58**, pp 6287 (1998).

- [72] F. Gazeau, C. Baravian, J.-C. Bacri, R. Perzynski, and M. I. Shliomis, "Energy conversion in ferrofluids: Magnetic nanoparticles as motors or generators," *Physical Review E*, Vol. **56**, pp 614 (1997).
- [73] H. Morimoto, T. Maekawa, and Y. Matsumoto, "Nonequilibrium Brownian dynamics analysis of negative viscosity induced in a magnetic fluid subjected to both ac magnetic and shear flow fields," *Physical Review E*, Vol. **65**, pp 061508 (2002).
- [74] V. M. Zaitsev, and M. I. Shliomis, "Entrainment of ferromagnetic suspension by a rotating field," *Journal of Applied Mechanics and Technical Physics*, Vol. **10**, pp 696 (1969).
- [75] A. Chaves, M. Zahn, and C. Rinaldi, "Spin-up flow of ferrofluids: Asymptotic theory and experimental measurements," *Physics of Fluids*, Vol. **20**, pp 053102 (2008).
- [76] C. Rinaldi, F. Gutman, X. He, A. D. Rosenthal, and M. Zahn, "Torque measurements on ferrofluid cylinders in rotating magnetic fields," *Journal of Magnetism and Magnetic Materials*, Vol. **289**, pp 307 (2005).
- [77] B. U. Felderhof, "Magnetoviscosity of a ferrofluid in an oscillating field," *Magnetohydrodynamics*, Vol. **37**, pp 307 (2001).
- [78] L. G. Leal, *Advanced transport phenomena: Fluid mechanics and convective transport processes* (Cambridge University Press, New York, 2007).